

DYNAMICS OF THE CLUSTER OF GALAXIES A3266 (SERCIC 40/6). I. SPECTROSCOPIC DATA

H. QUINTANA,^{1,2} A. RAMÍREZ,^{2,3} AND M. J. WAY⁴Astrophysics Group, Physics Faculty, P. Universidad Católica de Chile, Casilla 104, Santiago 22, Chile
Electronic mail: hquintana@astro.puc.cl

Received 1994 April 21; revised 1996 March 1

ABSTRACT

We present 387 velocities covering an area $1.8^\circ \times 1.8^\circ$, including 229 new galaxy velocities obtained from 309 spectra, of which 317 appear to be cluster members according to our analysis. Based on this extended velocity sample we reanalyzed the velocity structure of the cluster. We found a strongly decreasing velocity dispersion profile that, as well as the mean velocity, shows significant radial scatter. Inside the $2.5h_{50}^{-1}$ Mpc radius, the velocity dispersion has a value of 1306 ± 73 km s⁻¹, while further out than $3h_{50}^{-1}$ Mpc it falls below 800 km s⁻¹. The global dispersion is 1085 ± 51 km s⁻¹. We found a remarkable velocity substructure, which we interpret as a tidal outgoing arm reaching from the center to the northernmost extensions surveyed. The arm could be produced by a recent merger with another cluster, that moved from the front and SW direction and scattered from the main cluster core into the arm. This model allows us to derive an epoch for the collision between the more massive core and the front edge of the incoming cluster of $4 \times 10^9 h_{50}^{-1}$ yr ago and of $\sim 2 \times 10^9 h_{50}^{-1}$ yr for the merging of both cores. Formation of the dumb-bell is a later merger process of the two BCMs, consistent with theoretical estimates. The collision picture is also consistent with the distorted x-ray image. The very northernmost parts of the arm could, alternatively, be interpreted as ongoing infall of a few outlying loose groups. The suggestion of a faint galaxy system within $400h_{50}^{-1}$ kpc, satellite to the central dumb-bell, is maintained in spite of the large central velocity dispersion value; however, confirmation requires data for further compact faint members. From several mass estimators we derived a cluster dynamical mass value of $5 \times 10^{15} h_{50}^{-1} M_\odot$, but this value should be seen in the merger context described. © 1996 American Astronomical Society.

1. INTRODUCTION

Rich clusters of galaxies are objects of much interest in the study of the formation and evolution of large matter aggregates in the Universe. In all likelihood they are the largest bound masses now present. They have differing shapes, galaxy concentrations and populations. These differences are customarily interpreted as representing different stages in the gravitational matter evolution of the cluster. The most dense and possibly massive clusters are the most evolved. Many of them have galaxies of type cD at their centers. The view that such clusters have reached stationary equilibrium was generally accepted in the past, but the presence of substructures in these clusters weakens the virilization and relaxation hypothesis (Jones & Forman 1992; Miralda-Escudé 1993; Briel & Henry 1993; Salvador-Solé *et al.* 1993; Escalera *et al.* 1994).

The cluster A3266 (Abell *et al.* 1989), originally known as Seric 40/6, was one of the first discovered bright x-ray

sources in the southern skies, attracting the attention of researchers. The first evaluation of its large velocity dispersion was carried out by Melnick & Quintana (1981a and 1981b; hereafter referred to as MQ81a and MQ81b). Later studies by Materne *et al.* (1982), Carter *et al.* (1984), Hu *et al.* (1985), Quintana *et al.* (1985), Proust *et al.* (1987), Green *et al.* (1988), and Quintana & Ramírez (1990; hereafter referred to as QR90), confirmed a large velocity dispersion within the central $2.5h_{50}^{-1}$ Mpc. The central dumb-bell galaxy has been classified with cD characteristics and shows strong tidal distortions. The velocity difference between components of 350–400 km s⁻¹ leads one to wonder on the possibility that the pair is bound. Carter *et al.* (1985) have claimed detection of a rise in the internal velocities of the stellar population in the halo of both components, up to values of 600–700 km s⁻¹. QR90 suggested the probable presence of a satellite group of faint galaxies around the db, with a similar 700 km s⁻¹ velocity dispersion. In spite of such high dispersion, these authors favored a bound hypothesis for the central concentration as it smoothly joined the stellar dispersion and was consistent with a fairly high core mass.

The work by Teague *et al.* (1990; hereafter referred to as TCG90), published at the same time, does not address the presence of a central concentration. They reported a total of 146 radial velocities in the cluster (totalling 152 including previous literature values), out of which nearly 15% seem to be background. They used a multifiber spectrograph and a cross-correlation technique. A fairly large number of discrep-

¹Visiting Astronomer, Las Campanas Observatory of the Carnegie Institution of Washington.

²Visiting Astronomer, Cerro-Tololo Internamerican Observatory which is operated by the Association of Universities for Research in Astronomy, Inc. under contract with the National Science Foundation.

³Present address: Instituto Astronômico e Geofísico, University of São Paulo, Caixa Postal 9638 CEP 01065-970, SP. São Paulo, Brazil, Electronic mail: aramirez@vax.iagusp.usp.br

⁴Present address: Department of Physics and Astronomy, University of Missouri—St. Louis, 8001 Natural Bridge Rd., St. Louis, MO 63121-4499. Electronic mail: mway@newton.umsl.edu

ant redshifts was noticed by Fairall & Jones 1991 and assumed to be due to earlier unreliable data. When analyzing the present set of data, we also noticed an uncomfortable number of discrepant velocities in TCG90. Therefore, we have paid attention to the procedures employed to measure velocities, relying in ultimate circumstance in the capability of the (trained) eye to identify spectral features. Most of our velocities have been measured by “eye line identification” and by cross correlation. It is clear that cross correlation alone is not sufficient when the quality number “*R*” is less than 4 (as discussed in Sec. 3).

We present a deeper and wider study of A3266 to find whether subconcentrations were present which could indicate if the cluster is relaxed or not, and whether the velocity dispersion of A3266 is intrinsically high or just an artifact of important subclustering. As described below, we found an unusual velocity and spatial distribution that we interpret as evidence for a recent merger. We used several statistical tests as proposed in the literature (Bird 1994) to help in the determination of substructure, but found that most did not give an accurate estimate of what was obvious to us via a simple exploratory statistical analysis (Hoaglin *et al.* 1983), tailored to this problem. This points to the fact that some statistical tests used to quantify substructure must be used with care and that substructure features can hide from some global analysis. These detailed statistical tests as well as some simple featured *n*-body simulations will be presented in Paper II (Flores *et al.* 1996).

2. OBSERVATIONS

In this paper we report the results of two spectroscopic observing sessions aimed at obtaining better coverage of the velocity field of this cluster. Furthermore, we will include a remeasurement, using cross-correlation techniques, of our previously published digital spectra. The radial velocity coverage of this cluster is one of the highest. The $1.8^\circ \times 1.8^\circ$ area covered by the velocity measurement, at the redshift of A3266 corresponds to a square $11h_{50}^{-1}$ Mpc on a side (in units of $H_0 = 50h_{50}$ Mpc $^{-1}$ km s $^{-1}$, $h_{50} = 1$ and $q_0 = 1$ for numerical calculations, as assumed throughout). For comparison, at the distance of the Coma cluster, this distance would be a square 4.6° on a side.

2.1 Observations with the LCO 2.5 m Telescope Fiber Spectrograph

To explore the whole field covered by A3266, we used Steve Sheckman’s fiber spectrograph mounted on the 100” DuPont telescope at Las Campanas Observatory (LCO) on the nights of 1990 October 22–25, which were clear, dark, and had good seeing. The multifiber system consists of a plug plate at the focal plane to which 65 fibers are attached, and then run to a Boller and Chivens Spectrograph coupled to a 2*D*-Frutti detector (Sheckman 1989). Normally, 50–55 fibers were used for objects. Ten sky fibers were set aside and spaced at intervals of one every six fibers along the spectrograph. They were positioned in a more or less check-board pattern in the plug plate. The field coverage of the DuPont telescope is exceptional: a circle 2° in diameter or a

square 1.5° on a side. Allowing some overlap, with five fields we covered a field approximately $1.8^\circ \times 1.8^\circ$, centered on A3266. Exposure times were adjusted between 80 and 120 min, depending on the brightness of the selected galaxies for each of the exposures. Thus a total of 267 spectra in A3266 were obtained in this run (data on other clusters and groups are reported in separate publications). We used standard quartz lamp exposures of the dome to approximately correct for pixel-to-pixel variations of the 2*D*-Frutti detector. To properly illuminate the whole detector surface, the grating angle was changed to several values on these exposures. As well, helium-neon comparison lamp exposures were taken, off the windscreen, for wavelength calibration before and after each exposure. The 2*D*-Frutti detector has a small dark current and no corrections were made for that effect. With a 600 line mm $^{-1}$ grating plus the 2*D*-Frutti detector we cover ~ 3500 – 6900 Å, getting a dispersion of ~ 2.6 Å pixel $^{-1}$ and a resolution of ~ 10 Å.

2.2 Observation with Argus at CTIO

Observations were also carried out using the Argus spectrograph at the CTIO 4 m telescope during the early parts of two nights on 1990 February 17–19. Argus is a computer-controlled robot device that moves the fibers to the requested positions, allowing a traveling mirror to center the fiber on each object, if bright enough. The instrument had 19 working fibers, each associated to a companion sky fiber. An instrument failure, clouds on one night and poor seeing prevented the observation of the faintest galaxies surrounding the dumb-bell. However, three Argus fields were observed in A3266, securing some good spectra for a number of galaxies. The low success of this run prompted us to increase the fields observed at LCO, as previously described.

The Argus spectrograph with the CCD detector (the 800×800 pixels TI#2) located in the 4 m coude room has great stability. This was checked with He-Ar comparison lamps taken in the afternoon with the telescope pointing in quite different directions and from the lamps taken during the nights. We used grating KLGL2, tilted to provide a wavelength coverage from 3900 to 5600 Å, approximately. The preflashed CCD exposures were binned 2×1 in the fibers-slit direction, giving a dispersion of 2.2 Å pixel $^{-1}$ with a FWHM resolution of around 8 Å. Exposures of the A3266 fields were three times 900 s (each paused several minutes because of clouds) for the first field taken on the second night of the run, two 1800 s for the second field and two 1500 s for the third field, all taken on the final night. Because of the great wavelength stability exhibited by the instrument, we used a long comparison lamp taken every night with the telescope pointing to the zenith to calibrate all exposures in wavelength. To compare and check on possible zero-point shifts, we observed several velocities of standard stars and some galaxies with well-known radial velocities, using one of the fibers. Exposures of a white spot in the dome, of sunlight through a translucent white plastic block to diffuse the fibers shape (“milky”) and sky flats, were used to correct for pixel-to-pixel, large scale, and illumination variations of the CCD response. The projected fibers had a width from 2 to 4

pixels on the binned chip, while the cross shifts of the fiber images were no larger than 0.5 pixel due to telescope pointing changes.

2.3 Galaxy Positions

Positions in an area $1.8^\circ \times 1.85^\circ$ for 470 galaxies in A3266 were measured on the Optronics machine at ESO, Garching (a square of $12h_{50}^{-1}$ Mpc on a side at its redshift). We used a glass copy of the ESO Quick Blue Survey field 118, on which we measured the positions of all identifiable galaxies thought the monitor screen, while we scanned the plate by eye. Positions were obtained with reference to 32 astrometric standards from the Perth catalogue, using the standard programs available at ESO. We estimate the positions to be externally accurate to within 1.5 arcsec and within 0.3 arcsec internally. This is suitable for setting the fiber holes and for comparison to other work.

Positions of the fainter galaxies, particularly in the neighborhood of the central db galaxy were measured from a prime focus CTIO 4 m plate taken on IIIa-J emulsion, with reference to a large set of the galaxy positions already described.

3. REDUCTIONS AND RESULTS

Velocity determinations were carried out both using a cross-correlation technique and by identifying and fitting line profiles by eye. All reductions were performed within IRAF⁵ version 2.10.2. In particular, the packages LONGSLIT, HYDRA, ONEDSPEC, APEXTRACT, RV, and RVSAO (Kurtz *et al.* 1992) were used.

3.1 Reductions of LCO Fiber Frames

Due to the nature of the fiber+2D-Fruti system we had the typical S-shaped distortions inherent in this instrument. Therefore a six-order spline, three curve was used to trace our S-shaped spectra. As well, we sampled the spectra once every five pixels using the trace algorithm. This can catch discontinuities that are caused by the microchannel and image intensifiers of the 2D-Fruti or the twisting of the fibers in their casings. To obtain a proper sky subtraction one needs to know the transmission in each fiber, which can normally be done via sky flats, but the fiber+2D-Fruti system is not sufficiently stable that we can use one sky flat per night. For example, we found that the position of the spectra on the 2D-Fruti detector was variable depending upon where the telescope was pointing. This is most likely due to changing magnetic fields in the dome which seem to affect the 2D-Fruti detector greatly. Because of this effect and because the sky fibers were plugged in different free holes on each field causing their illumination or fit in the holes to vary from exposure to exposure, we would have needed one sky flat for each of the three fields observed per night, immediately after each object exposure. Since this is not practically possible

we took another route which we believe is good to $\pm 5\%$. We measured the flux of the 5577 Å sky line in each of the object exposures. Typically the object spectra intensity are less than 5% of this sky line. With this measurement we then had a measure of the fiber-to-fiber transmission or flux which we put in a “fiber transmission table” for later use. The HYDRA package was used to extract the spectra, correct pixel-to-pixel variations via the dome flat, use the fiber transmission table for appropriate sky subtraction, and put the spectra on a linear in wavelength scale. The wavelength solutions for 20–30 points using a 3–6 order Chebyshev typically yielded residual values less than 0.5 rms Å, where 1 pixel ~ 2.6 Å. The ten sky spectra were combined via a median filter.

Three different methods were used to measure the redshift of the objects. For normal early-type spectra, we were able to use two different cross-correlation algorithms now currently supported inside of IRAF (RV and RVSAO). For nonearly-type spectra (i.e., emission lines, E+A, etc.) we resorted to a line-by-line Gaussian fit. Normally a low R value ($R \leq 4$) (Tonry & Davis 1979; hereafter referred to as TD79) would indicate a need to look at the spectra and try line-by-line Gaussian fitting. For a description of the cross-correlation algorithm and the Tonry & Davis R number, see TD79. Prior to cross correlation, the spectra were continuum subtracted, and filtered in Fourier space with a ramp filter, to remove high-frequency noise and low-frequency trends not removed by continuum subtraction. Filtering in Fourier space (similar to smoothing in real space) has the advantage of not introducing phase shifts, which can occur when smoothing the data in real space. Several different combinations of radial velocity templates were tried, some of which include: an average of four templates, using only a synthetic template, and using the template that gives the lowest error value out of four templates. Of the four templates used two were galaxy spectra taken with the fiber instrument, NGC 1407 and NGC 1426, one was from the previous spectrograph on the 2.5 m at Las Campanas (Spectograph) NGC 1700, and one was a synthetic template. The synthetic template was constructed from the library of stellar spectra of Jacoby *et al.* (1984). We used ratios of stellar light synthesized for the E0 galaxy NGC 1374 from the synthesis studies of Pickles (1985). In the end we decided that the template, which gave the lowest error value out of the four templates mentioned above, proved to have more consistent results.

By obtaining velocities from two different cross-correlation algorithms (RV and RVSAO) we have a check on the reliability of each program. In general, the difference between RV and RVSAO dropped as we went to higher R values (see Fig. 1). Part of the reason for the difference between the two programs was related to different parameter files for each. For example, picking the exact number of log bins to rebin the data in prior to cross correlation (not supported in RV), amongst other parameters, exist between the two programs and are the most likely cause of the velocity difference spread seen in Fig. 1. We noted a mean velocity shift between the two programs of ~ 8 and 73 km s^{-1} rms, well within 1σ .

⁵IRAF is distributed by NOAO, which is operated by the Association of Universities for Research in Astronomy Inc., under contract with the National Science Foundation.

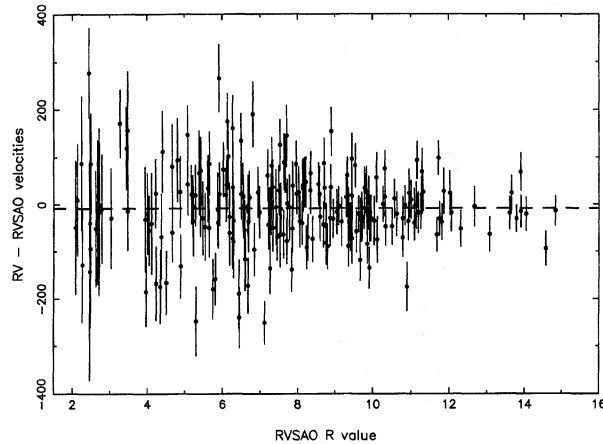


FIG. 1. Residuals of RV vs $RVSAO$. The thick dotted line represents a zeroth-order polynomial fit through the data plus a 3σ clip which corresponds to an average shift of $\sim 8 \text{ km s}^{-1}$ with an rms of $\sim 73 \text{ km s}^{-1}$.

3.2 Reductions of the Argus Observations

The Argus reductions proceeded along the same lines as the fiber data, but the one-dimensional spectra is simpler. The transmission of object and sky fibers were determined and the sky subtracted using the transmission corrected sky spectra adjacent to each object. For wavelength calibration, we used a Legendre polynomial of order 8 based on 20 lines (on average) using He-Ar comparison spectra. Distortions at both ends of the chip forced the use of a polynomial order higher than fourth. The first velocity measurements were done by identifying the lines, normalizing the spectra and applying a Gaussian fit to the lines.

All spectra, objects, and templates had the same initial wavelength 3881 \AA and final wavelength 5900 \AA and were rebinned to a log-linear dispersion: $2.2 \text{ \AA pixel}^{-1}$. To select the best templates, each of our candidate templates were correlated against all candidate templates. Only high signal/noise templates with consistent velocity results were kept and used for the cross-correlation program.

With seven templates our objects were cross correlated automatically using $RVSAO$. Similar filtering was applied as described in Sec. 3.1. Cross-correlation peak fitting was performed by using a parabola. The final velocities were computed with heliocentric corrections and were corrected for the templates relative velocities. We took the three (out of seven) velocities with the highest R values, that corresponded to the line by line determined values, to compute the final velocity with. Furthermore, if the values from the seven templates were not consistent, we used the template with the highest R value or used the cross correlation interactively looking for the peak at the velocity position expected from the line-by-line Gaussian fitting by eye. If no peaks were detected in the cross-correlation plot, but spectral lines were observed, the velocity was measured from the mean of ~ 5 spectral lines fitted by a Gaussian function to measure their center position. As with the fiber data, fitting a Gaussian function to spectral features was used to measure the velocity of spectra with strong emission lines.

3.3 Schematic Data Remeasurements

In order to complete the velocity data on a homogeneous basis, we remeasured our previously published values (QR90), observed with the two-channel intensified reticon detector (Schematic) on the 2.5 m DuPont telescope, using the same Boller and Chivens spectrograph used in the fiber sessions described above. All spectra, objects, and templates, had the same initial and final wavelengths ($3510\text{--}6800 \text{ \AA}$) and were rebinned to a log-linear dispersion: $1.4 \text{ \AA pixel}^{-1}$. To select the best templates, all templates were correlated against each other. Only eight high signal/noise spectra with consistent velocity results were considered good enough for our purposes. With these templates our objects were cross correlated automatically using $RVSAO$. Final velocities were calculated following the same methods used with the Argus data.

3.4 Results

A total of 309 new spectra were obtained, 263 from the five DuPont fiber fields and 46 from the Argus instrument. For 13 galaxies we obtained 2 fiber spectra and 1 galaxy was observed in 3 fibers. Three stars were found among the more compact objects measured (one, No. 25804, was given a 63752 km s^{-1} velocity by TCG90). 55 values were remeasured from the Schematic data. Table 1 gives these results, where column 1 shows our identification number, columns 2 and 3 give 1950.0 epoch positions, and columns 4, 5, and 6 give the individual velocities, their errors (1σ), the corresponding R Tonry and Davis values, the number of measured lines (mostly emission) if the R number was too low for a proper velocity determination, and a ‘e’ comment showing the presence of emission lines. Here we have integrated velocity values from the literature, as described in the next section. Columns 7 and 8 give a code for the observation source or references, as indicated in the notes at the end of the table, and the fiber or galaxy number in the reference. If we found a discrepant or very uncertain value, we did not use that velocity in our calculations. This is indicated by a negative sign in the previous column. Columns 9 and 10 give the adopted final velocities and their derived errors in these calculations if they are a combination of several values or if they have been shifted, as discussed below. For future reference note that we do not include any velocities of our own in Table 1 with an R value less than 4 unless it has been verified by a line-by-line identification of the spectrum. We would also like to note that we believe the velocity errors as given by $RVSAO$ underestimate the true error by $\sim 30\%$. This can be seen by the high rms values shown in the comparisons of measurements of the same object thru different instruments as described next.

We obtained velocities from three instruments on two telescopes. Before we can combine the data, it is necessary to analyze possible systematic shifts and correct the values accordingly; otherwise, a dynamical analysis can be spuriously influenced, resulting in too large a velocity dispersion value. Fortunately, the two larger sets of data came from the DuPont telescope, the same Boller and Chivens spectrograph

TABLE 1. A3266—Velocities.

Ident.	α (1950)	δ (1950)	v_{\odot}	err	R	Ref	Id.Ref	\bar{v}_{\odot}	err
27020	4 23 12.8	-60 47 43.3	18539	54	4.0	fibr	1045		
27017	4 23 26.0	-61 22 12.0	17015	38	7.5	fibr	1343		
27018	4 23 27.7	-61 09 59.8	17120	45	5.7	fibr	1044		
27036	4 23 39.5	-62 23 49.3	5339	50	4.5	fibr	430		
27031	4 23 39.6	-61 30 52.1	17547	61	3	e fibr	1330		
27034	4 23 42.8	-62 11 01.4	18215	39	7.4	fibr	429		
27023	4 23 50.9	-60 56 02.3	19044	122	3.1	fibr	444		
27024	4 23 52.9	-60 56 12.5	17873	88	3.7	fibr	1344		
27029	4 24 01.1	-61 12 01.6	17373	64	4.0	fibr	1342		
27022	4 24 03.4	-60 52 46.6	18088	41	6.5	fibr	1345		
27039	4 24 03.9	-61 46 15.6	17320	200	1	fibr	1331		
27037	4 24 04.4	-62 10 24.7	5627	95	2.6	fibr	1329		
27045	4 24 06.9	-60 54 34.1	18443	58	5.2	fibr	1046		
27043	4 24 14.1	-61 04 29.0	17620	68	4.6	fibr	1341		
27042	4 24 15.8	-61 12 23.1	5487	39	5.6	fibr	1340		
27047	4 24 24.4	-60 54 03.1	18576	56	4.4	fibr	1346		
27044	4 24 26.8	-61 02 02.5	29125	57	6.0	fibr	445		
27041	4 24 29.4	-61 18 17.1	17262	24	12.1	fibr	443	17253	30
			17230	41	7.7	fibr	1339		
27059	4 24 38.9	-62 07 19.1	17113	43	6.4	fibr	1026		
27055	4 24 42.7	-61 19 44.2	17488	36	8.3	fibr	1338		
27057	4 24 50.7	-61 30 09.4	23118	86	3.7	e fibr	1246		
27054	4 24 52.2	-61 18 53.2	17093	32	10.0	fibr	1043		
27053	4 24 54.2	-61 17 00.1	17461	41	7.6	fibr	1337		
27052	4 24 56.4	-61 03 25.8	18384	51	5.7	fibr	1336		
27067	4 25 04.2	-60 43 34.4	18177	41	6.1	fibr	1347		
27063	4 25 07.0	-61 15 53.0	5498	102	5	e fibr	1247		
27064	4 25 14.5	-61 15 45.0	17165	51	6.0	fibr	1042		
27062	4 25 25.5	-61 27 03.8	17234	65	3.9	fibr	1027		
27075	4 25 29.6	-60 59 43.3	27558	123	4	e fibr	1348		
27072	4 25 41.9	-60 50 31.2	21402	50	4.0	fibr	1349		
27076	4 25 43.5	-61 27 42.8	17167	42	6.9	fibr	1028		
27074	4 25 44.2	-60 55 00.1	29437	60	4.7	fibr	1350		
27083	4 25 56.1	-61 24 41.4	17191	62	5.0	fibr	731		
27085	4 25 57.7	-61 18 54.2	16964	60	5	e fibr	1335		
27086	4 26 04.8	-60 58 09.9	17330	50	2	e fibr	1352		
27082	4 26 15.3	-61 33 13.2	17236	100	3	fibr	1332		
27080	4 26 15.9	-61 58 60.0	18008	48	6.1	fibr	1025		
27079	4 26 18.0	-62 20 33.1	17137	69	5	e fibr	428		
27091	4 26 22.6	-61 05 39.9	17991	45	7.0	fibr	1041		
27094	4 26 27.7	-61 39 22.7	27520	38	7.3	fibr	442		
27092	4 26 32.1	-61 10 43.7	18411	28	12.4	fibr	446	18415	30
			18426	44	8.4	fibr	1040		
27090	4 26 38.2	-60 58 30.1	18097	54	4.5	fibr	747		
27095	4 26 39.6	-62 17 06.5	17594	34	8.2	fibr	1234		
27093	4 26 41.2	-61 20 43.1	17579	30	9.8	fibr	441	17581	30
			17586	46	6.4	fibr	1039		
27104	4 27 00.7	-61 19 13.7	17849	45	5.4	fibr	1245		

fitted with the same grating and fairly similar detectors (both use the same Carnegie image tube as the first stage). The main difference comes from the light feed to the spectrograph. Therefore, one should expect small systematic differences between the old Sheckograph and the new fiber data. We have eight spectra in common with the A3266 data (rather a small number). The mean difference is 4 km s^{-1} with a dispersion of 40 km s^{-1} . This is negligible and well

within individual errors, so both sets can be treated as one. Between the Campanas 2.5 m (Sheckograph+Fibers) and the Argus data we have 12 spectra in common, plus 17 from Quintana *et al.* (1995a), and 7 from Ramirez (1994). This gives us a mean difference of 76 km s^{-1} and a rms of 161 km s^{-1} for the 36 that were within a 3σ clip of the data used to remove a few widely discrepant points. The large rms implies an uncertain shift. However, when comparing the

TABLE 1. (continued)

Ident.	α (1950)	δ (1950)	v_{\odot}	err	R	Ref	Id.Ref	\bar{v}_{\odot}	err
27102	4 27 03.9	-61 20 17.9	17939	32	8.1	fibr	746		
27096	4 27 04.3	-62 26 40.8	18545	36	7.3	fibr	1233		
27099	4 27 04.5	-61 25 29.6	22890	45	5.6	fibr	-440	17078	30
			17078	23	8	shec	368		
27103	4 27 05.6	-61 19 42.4	17977	30	9.2	fibr	439		
27108	4 27 06.4	-61 03 11.3	22923	59	4.2	fibr	1038		
27107	4 27 07.2	-61 14 50.0	16770	40	7.4	fibr	1334		
27106	4 27 10.2	-61 17 43.0	18666	44	4.7	fibr	447		
27101	4 27 13.4	-61 20 33.3	16700	77	3.3	fibr	1037		
27098	4 27 15.2	-61 39 09.2	17155	35	8.7	fibr	438	17148	30
			17144	29	10.9	shec	844		
27097	4 27 20.8	-62 12 12.1	18395	31	9.9	fibr	427		
27118	4 27 23.8	-61 06 54.3	18421	47	5.6	fibr	448		
27112	4 27 24.8	-60 42 54.5	17541	88	4	e fibr	1353		
27130	4 27 24.8	-62 20 49.5	16630	37	6	e fibr	426		
27127	4 27 25.3	-62 05 49.0	16862	85	3.1	fibr	1024		
27128	4 27 25.7	-62 05 56.6	17008	90	2.9	e fibr	730		
27120	4 27 28.1	-61 13 31.2	18893	44	5.9	fibr	1248		
27124	4 27 29.7	-61 24 45.9	16599	23	7	shec	341		
27122	4 27 33.9	-61 16 43.5	19773	28	9.8	fibr	449		
27119	4 27 37.0	-61 09 28.4	17890	40	6.3	fibr	450		
27121	4 27 40.3	-61 15 12.9	22800	73	2.3	fibr	745		
25470	4 27 41.2	-61 28 48.4	29371	56	4.0	argu			
27125	4 27 42.9	-61 48 09.7	18947	62	3.1	fibr	1333		
27143	4 27 50.2	-60 56 48.3	21295	49	5.5	fibr	1047		
27139	4 27 50.4	-61 10 27.4	16803	38	8.9	fibr	1036		
25276	4 27 53.2	-61 22 21.5	15824	35	9.1	fibr	1035		
27135	4 27 53.5	-61 53 20.1	18403	32	9.7	fibr	1023		
27131	4 27 55.7	-62 22 31.5	17852	54	4.2	fibr	1232		
25150	4 27 58.7	-61 18 05.6	16497	38	8.5	fibr	437		
25275	4 27 59.0	-61 21 51.9	15847	45	5.7	argu			
25679	4 28 01.7	-61 34 13.2	17390	82	2.9	argu		17339	37
			17312	47	7.0	shec	679		
			17263	91	4.2	TCG90	220		
27138	4 28 01.9	-61 31 37.6	17564	52	5.1	shec	587	17593	39
			17515	62	6.6	TCG90	219		
27132	4 28 02.4	-62 20 41.3	17054	38	5	e fibr	425		
27140	4 28 02.4	-61 04 22.5	18277	43	7.2	fibr	1034		
27136	4 28 07.7	-61 37 23.0	16476	48	5.8	fibr	436		
27148	4 28 08.6	-60 42 55.4	19395	39	8.1	fibr	1048		
27154	4 28 15.5	-60 55 31.0	18470	40	5.9	fibr	452		
27159	4 28 16.9	-61 07 32.2	17179	35	7.4	fibr	744		
25122	4 28 21.1	-61 17 06.4	16683	46	5.5	fibr	743	16676	41
			16644	100	2.2	argu			
27165	4 28 21.9	-61 30 46.0	15928	51	4.2	fibr	1244		
25194	4 28 24.0	-61 19 30.8	18983	93	2.8	e fibr	742	19032	76
			19012	132	3.6	TCG90	201		
27160	4 28 24.2	-61 08 30.5	19486	52	5.7	fibr	1249		

whole data set with the literature, as done in the next section, a better determination can be made.

3.5 Comparison with the Literature

Several authors have measured velocities in A3266, as indicated in the introduction. The older data were reviewed by QR90. The largest published set of velocities is by TCG90. We take into account data in common with these

authors to establish a shift between the data sets. In fact, besides the data of this paper, we have in common 150 other velocities, in the clusters A3558, A3391, and A3395 (Quintana *et al.* 1995b; Ramirez 1994). Excluding discrepant values, we have 40 galaxies in common with TCG90 with fibers, 120 with Schectograph, 62 with Argus, and 21 with 2D-Fruti. The mean differences between sets are -102 ± 23 , -133 ± 14 , -136 ± 15 , and -139 ± 39 km s⁻¹, respectively.

TABLE 1. (continued)

Ident.	α (1950)	δ (1950)	v_{\odot}	err	R	Ref	Id.Ref	\bar{v}_{\odot}	err
27153	4 28 25.7	-60 52 53.2	19248	73	4.5	fibr	1049		
27169	4 28 26.1	-62 10 43.3	16755	43	5.6	fibr	1022		
27151	4 28 26.5	-60 43 29.4	18090	40	3	fibr	1354		
27157	4 28 27.7	-60 59 36.2	17973	55	4.9	fibr	453		
27156	4 28 29.8	-60 56 46.9	19145	56	4.9	fibr	748		
27152	4 28 30.2	-60 52 38.2	19359	51	5.0	fibr	749		
25732	4 28 31.0	-61 35 45.4	19321	44	5.0	shec	732	19346	46
			19313	82	4.8	TCG90	222		
27155	4 28 33.3	-60 56 18.8	17990	72	4.4	fibr	1355		
25648	4 28 33.6	-61 32 58.7	18378	35	9.2	fibr	732	18331	30
			18320	28	9.1	shec	648		
			18171	42	7.2	TCG90	180		
27158	4 28 33.7	-61 03 57.0	18342	89	4	e fibr	1033		
27168	4 28 34.2	-62 08 01.8	16877	63	5.0	e fibr	1328		
25393	4 28 36.2	-61 26 20.9	18323	55	4	e fibr	733		
25174	4 28 36.3	-61 18 35.4	17137	30	10.5	fibr	435	17137	30
			17341	105	3.5	TCG90	-196		
27162	4 28 36.6	-61 10 06.2	16251	34	7.8	fibr	1032		
25217	4 28 37.7	-61 20 29.7	17656	43	4.7	argu		17667	60
			17900	110		M082			
			17460	83	4.7	TCG90	197		
25240	4 28 37.8	-61 20 46.9	19953	44	6.2	argu		19959	40
			20000	110		M082			
25365	4 28 44.1	-61 25 33.5	17297	39	7.6	fibr	1031	17317	30
			17292	51	4.1	argu			
			17268	55	7.7	TCG90	185		
25620	4 28 44.8	-61 32 30.6	17158	79	3.7	shec	620	17127	56
			16974	82	4.8	TCG90	179		
28016	4 28 45.9	-61 40 14.2	17684	123	2.9	TCG90	104	17804	123
27167	4 28 46.3	-61 50 57.9	49405	50	6.0	fibr	431		
27176	4 28 47.0	-60 57 38.5	17161	57	5.0	fibr	1351		
27173	4 28 47.6	-61 30 04.2	19134	38	7.5	fibr	1243	19115	30
			19095	30	8.0	shec	7173		
			19041	69	5.8	TCG90	181		
25997	4 28 47.8	-61 47 12.4	19723	42	8.2	fibr	1029	19800	43
			19741	44	9.8	TCG90	94		
			19833	50		MQ81a	8		
27170	4 28 49.0	-62 20 15.7	5839	33	8.6	fibr	1231		
25870	4 28 50.1	-61 40 56.7	19843	55	3.8	shec	870	19838	48
			19702	99	3.8	TCG90	93		
25146	4 28 51.7	-61 17 51.5	17059	35	9.5	fibr	434	17065	33
			16998	103	3.6	TCG90	194		
25253	4 28 51.7	-61 21 19.5	17225	75	3.3	argu		17231	47
			16862	300		MQ81a	-9		
			17116	61	6.5	TCG90	200		
28044	4 28 53.0	-61 28 06.2	16683	81	4.8	TCG90	182	16803	81
25171	4 28 53.3	-61 18 56.3	19872	45	7.2	fibr	1250	19886	40
			19675	80		MQ81b	-28		

This comparison confirms the consistency between the Schectograph, Argus, and fiber data. It is clear there is a shift between TCG90 and us. Therefore, we applied to their data a shift of 120 km s^{-1} , to combine the data sets.

We found ourselves in gross disagreement with most of those velocities noted as uncertain by TCG90 with R values less than 2.5 (see Figs. 2 and 3), we denote these by an

asterisk in front of the TCG90 reference in our table. The largely discrepant velocities were mostly attributed by TCG90 to be background galaxies, while we put them in the cluster. This confirms that TCG90 velocities with R less than 2.5 are unreliable and are only used in this paper when confirmed by another measurement. In Figs. 4 and 5 we show two of our typical LCO fiber spectra, one with a high and

TABLE 1. (continued)

Ident.	α (1950)	δ (1950)	v_{\odot}	err	R		Ref	Id.Ref	\bar{v}_{\odot}	err
			19823	88	4.4		TCG90	199		
25700	4 28 54.8	-61 34 30.6	18417	63	3.5		argu		18477	34
			18497	36	10.1		shec	700		
28028	4 28 54.8	-61 39 37.7	75798	161	2.0	*	TCG90	-135		
28017	4 28 54.9	-61 40 09.9	16491	145	2.3		TCG90	-105		
25121	4 28 58.3	-61 17 01.0	19948	47	7.7	e	fibr	741	19969	32
			20000	50			MQ81b	27		
			19816	123	2.9		TCG90	193		
27172	4 29 03.0	-61 55 33.5	17000	56	5.5		fibr	432		
26057	4 29 03.1	-61 49 16.8	17467	38	6.5		shec	1057	17497	49
			17458	62	6.6		TCG90	100		
27174	4 29 03.5	-61 21 22.2	17532	82	4	e	fibr	1242		
25916	4 29 04.7	-61 43 24.7	17569	45	5.1		shec	916	17579	36
			17478	61	6.8		TCG90	77		
26086	4 29 04.9	-61 51 16.6	19689	39	6.6		fibr	1021		
25789	4 29 05.1	-61 37 21.3	16363	77	4.1		shec	789	16430	41
			16336	47	9.0		TCG90	177		
27177	4 29 06.2	-60 52 55.0	19697	35	8.4		fibr	1050		
28020	4 29 09.6	-61 43 58.6	15622	80	2.1	*	TCG90	-110		
25144	4 29 09.8	-61 17 52.9	17626	94	4.0		TCG90	192	17745	94
28021	4 29 12.8	-61 45 57.3	17462	70	5.7		TCG90	111	17582	70
25289	4 29 13.1	-61 23 13.6	17830	30	9.7		fibr	1241	17837	30
			17780	86	4.5		TCG90	186		
25547	4 29 13.2	-61 30 46.0	19046	49	5.2		shec	547	19041	42
			18906	89	4.3		TCG90	175		
28019	4 29 13.3	-61 39 30.7	16702	119	3.0		TCG90	109	16822	119
25390	4 29 13.9	-61 26 15.6	19073	36	7.4		argu		19058	37
			18841	93	4.1		TCG90	170		
27171	4 29 14.6	-62 23 01.7	24747	130	3.1	e	fibr	1230		
25617	4 29 14.7	-61 32 48.9	17152	48	5.8		shec	617		
28022	4 29 14.9	-61 46 33.4	57017	125	2.8		TCG90	112	57137	125
27182	4 29 19.0	-61 31 21.9	16015	112	5	e	fibr	433		
27183	4 29 19.0	-61 37 30.8	15470	49	5.2		fibr	1240		
25075	4 29 21.5	-61 14 50.0	17791	38	6.4		argu		17769	42
			17565	76	5.2		TCG90	191		
28042	4 29 27.2	-61 26 28.9	16647	103	3.6		TCG90	168	16767	103
28043	4 29 27.2	-61 31 54.1	17903	127	2.7		TCG90	172	18023	127
25103	4 29 31.6	-61 16 05.9	19595	95	2.1		fibr	1252	19595	95
			45441	150	2.2	*	TCG90	-188		
27181	4 29 32.1	-61 12 33.3	17642	38	7.8		fibr	1030	17677	77
			17729	84	4.7		TCG90	190		
27184	4 29 33.0	-62 15 08.1	8638	74	3.6		fibr	1229		
28018	4 29 33.7	-61 39 12.8	17487	167	1.8		TCG90	-108		
25072	4 29 35.0	-61 14 59.9	18932	35	7.2		fibr	454	18883	32
			18804	54	4.7		fibr	1253		
			18844	73	2.8		argu			
			18728	88	4.4		TCG90	189		
25812	4 29 35.1	-61 38 09.3	16902	66	4.4		shec	812	17042	228

another low value of R . In Figs. 6 and 7 we also show Argus and Schectograph spectra.

For references other than TCG90 we have too few common velocities to obtain meaningful shifts. All other data are consistent with quoted errors and zero shifts (MQ81a, 4 values; MQ81b, 14 values; Materne *et al.* 1982, 2 values; Green *et al.* 1988, 5 values; Vidal 1975, 2 values).

3.6 Final Average Velocities

When galaxies had more than one velocity (and we have numerous values in the literature as well), we adopted as the final value the weighted mean velocity and their attached uncertainty. Weighted factors came from the references published uncertainties and our internal uncertainties, which are

TABLE 1. (continued)

Ident.	α (1950)	δ (1950)	v_{\odot}	err	R	Ref	Id.Ref	\bar{v}_{\odot}	err
			17108	76	5.2	TCG90	70		
28007	4 29 38.9	-61 41 33.6	18390	122	2.9	TCG90	73	18510	122
28013	4 29 40.1	-61 44 13.6	16774	107	3.4	TCG90	96	16894	107
25725	4 29 41.7	-61 35 12.4	19509	41	7.5	shec	725	19509	41
			25768	84	2.1	TCG90	-12		
25822	4 29 42.5	-61 38 24.3	16701	69	3.8	argu		16704	30
			16586	38	5.8	TCG90	6		
			16869	144		W080			
			16630	100		MQ81a			
			16681	134		G088			
25644	4 29 44.5	-61 33 24.2	17995	42	8.3	shec	644	17994	42
			44581	72	2.6	TCG90	-13		
27186	4 29 45.0	-62 23 08.4	18661	50	6.5	fibr	1228		
28011	4 29 46.9	-61 41 49.1	60842	136	2.5	TCG90	-92		
25783	4 29 47.1	-61 36 54.9	17264	62	5.2	shec	783	17264	62
			43943	91	1.9	* TCG90	-15		
25675	4 29 49.2	-61 34 21.5	18382	52	5.9	shec	675	18402	41
			18319	69	2.8	TCG90	56		
27188	4 29 49.4	-61 53 37.4	19015	41	8.2	fibr	729	19020	37
			18925	90	4.3	TCG90	228		
28012	4 29 50.0	-61 45 56.4	18276	83	4.7	TCG90	95	18396	83
25412	4 29 50.1	-61 26 46.2	17471	82	2.7	fibr	734	17582	184
			17768	136	2.5	TCG90	164		
28014	4 29 53.9	-61 44 19.2	19480	91	4.2	TCG90	99	19600	91
27192	4 29 56.6	-61 00 10.9	18594	74	3.0	fibr	1254	18565	49
			18542	66	3.9	fibr	1301		
27189	4 29 58.0	-61 35 25.3	18522	41	6.5	fibr	1239	18522	41
			53328	107	1.6	* TCG90	-26		
28015	4 29 59.0	-61 49 12.5	16958	186	1.6	TCG90	-102		
25697	4 29 59.2	-61 34 60.0	20049	65	5.2	shec	697	20049	65
			26473	81	2.2	TCG90	-16		
25696	4 30 00.1	-61 34 43.2	18408	41	8.0	shec	696		
25883	4 30 00.3	-61 41 30.5	15727	36	7.7	fibr	1238	15727	32
			15603	82	4.8	TCG90	74		
25284	4 30 01.3	-61 23 32.5	16667	37	7.8	fibr	1237	16653	34
			16455	88	4.4	TCG90	162		
25500	4 30 01.6	-61 29 05.4	16520	130	1.7	argu		16557	95
			16600	140	2	MQ81a	5		
			43435	79	2.3	* TCG90	-21		
25672	4 30 02.0	-61 33 37.7	18916	63	5.1	shec	672	18872	38
			18930	200		MQ81b	25		
			18721	50	4.2	TCG90	14		
25136	4 30 05.2	-61 17 54.1	16173	32	9.8	fibr	416	16188	36
			16153	75	5.3	TCG90	159		
25524	4 30 05.2	-61 29 57.6	18815	33	8.6	shec	524	18819	30
			18719	70	2.7	TCG90	20		
28025	4 30 06.0	-61 39 23.4	15134	120	3.0	TCG90	115	15254	120
28027	4 30 06.2	-61 48 52.3	37281	70	3.9	TCG90	103	37401	70

given by IRAF, using the formula $\sigma_{\text{int}}=0.75W/(1+R)$, where R is the Tonry–Davis number, and W the FWHM of the parabola used to fit the correlation peak.

The error of the weighted mean $\sigma_{\mu}=\sigma/\sqrt{N}$, depends upon whether we assumed all velocities (ours and those in the literature) believable. If this is so, then we use $\sigma_{\mu\text{err}}$. If we assumed the quoted velocity errors to be only weights and not to represent the physical velocity errors, the uncertainty

of the weighted mean is given by the weighted rms dispersion $\xi_{\mu W}$, where

$$\sigma_{\mu\text{err}} = \frac{1}{\sqrt{\sum_i (1/\sigma_i^2)}}$$

and

TABLE 1. (continued)

Ident.	α (1950)	δ (1950)	v_{\odot}	err	R	Ref	Id.Ref	\bar{v}_{\odot}	err
28023	4 30 06.3	-61 41 46.0	30602	109	1.4	TCG90	-114		
25882	4 30 06.5	-61 42 00.5	18065	44	6.0	fibr	735	18062	38
			17934	84	4.6	TCG90	76		
25269	4 30 09.4	-61 22 05.0	17098	29	8.2	argu		17083	32
			16893	63	6.5	TCG90	161		
27197	4 30 09.4	-60 53 02.7	18692	43	7.0	fibr	1303		
27200	4 30 09.5	-61 00 41.6	18827	75	3.0	fibr	1302		
27198	4 30 10.1	-60 54 38.9	18345	35	8.7	fibr	750		
25114	4 30 10.2	-61 17 21.2	18101	51	4.5	argu		18059	30
			18033	37	6.8	argu			
			17952	67	6.1	TCG90	158		
25719	4 30 10.6	-61 35 34.6	18208	49	6.0	shc	719	18228	42
			18170	86	3.1	TCG90	19		
25133	4 30 10.8	-61 17 58.1	17186	40	6.8	argu		17147	46
			13605	90		MQ81a	-10		
			16972	48	8.8	TCG90	160		
28051	4 30 11.5	-61 32 55.1	17077	118	3.0	TCG90	284	17197	118
28050	4 30 11.6	-61 33 32.7	63510	171	1.8	*	TCG90	-283	
25966	4 30 12.5	-61 45 44.5	19809	77	3.4	TCG90	97	19929	77
25694	4 30 12.6	-61 34 35.1	15371	57	4.2	shc	694	15452	102
			15460	71	2.7	TCG90	17		
25070	4 30 12.7	-61 14 48.4	18351	35	7.0	argu		18359	31
			18280	78	5.1	TCG90	154		
25435	4 30 13.9	-61 27 24.3	18627	42	7.1	fibr	1010	18627	42
			35110	78	2.4	TCG90	-50		
28052	4 30 14.1	-61 36 27.5	71867	169	1.8	*	TCG90	-285	
27203	4 30 14.2	-61 13 04.4	18566	40	7.2	fibr	1255	18555	38
			18336	126	2.8	TCG90	153		
25382	4 30 15.2	-61 26 35.2	16720	57	4.9	shc	382		
27199	4 30 15.5	-60 59 27.6	18903	44	6.1	fibr	752		
28049	4 30 16.7	-61 28 09.4	17223	114	3.1	TCG90	279	17343	114
25671	4 30 16.8	-61 33 59.0	18565	93	2.6	shc	671	18341	357
			17936	105	3.0	TCG90	282		
28002	4 30 16.8	-61 34 58.4	27207	100	1.6	*	TCG90	-54	
25820	4 30 17.1	-61 38 51.0	20079	33	7.9	shc	820	20035	51
			20340	110		M082	-		
			19854	39	5.0	TCG90	37		
28057	4 30 17.1	-61 35 21.0	17205	66	3.0	TCG90	18	17325	66
25100	4 30 17.4	-61 16 15.9	17917	42	5.7	argu		17932	45
			17942	120	3.0	TCG90	156		
25819	4 30 17.4	-61 38 22.9	19682	64	4.3	argu		19718	30
			19609	22	7.2	TCG90	5		
			19703	79		G088			
			19600	130		MQ81b	11		
			20210	110		M082	-		
27194	4 30 17.4	-60 41 49.1	7028	35	7	e	fibr	1304	
25640	4 30 17.8	-61 32 57.9	18440	64	5.2	shc	640	18525	97
			18516	73	2.6	TCG90	34		

$$\sigma_{\mu W} = \sqrt{\left(\frac{\sum_i w_i V_i^2}{\sum_i w_i} - \bar{V}^2\right) * \frac{1}{N-1}},$$

where

$$w_i = \frac{1}{\sigma_i^2}.$$

If internal uncertainties adequately measure the external uncertainties, and if the number of individual measurements is large, both ways should give the same results in the mean, but $\sigma_{\mu \text{err}}$ is too low if internal uncertainties underestimate external ones, and $\sigma_{\mu W}$ is too low if by chance the measured values are close to each other.

We therefore adopt the larger of both estimates, unless the

TABLE 1. (continued)

Ident.	α (1950)	δ (1950)	v_{\odot}	err	R		Ref	Id.Ref	\bar{v}_{\odot}	err
28024	4 30 18.2	-61 37 36.1	63081	197	1.4	*	TCG90	-106		
25879	4 30 19.1	-61 41 57.3	17142	105	3.0		argu	-	18612	62
			18492	62	6.6		TCG90	75		
27202	4 30 19.3	-61 05 34.5	17980	38	5	e	fibr	740		
27195	4 30 19.8	-60 48 22.0	18422	54	4.2		fibr	753		
25718	4 30 20.0	-61 35 20.8	17359	56	4.4		argu		17351	46
			17365	120			MQ81b	26		
			17310	110			M082			
28000	4 30 20.4	-61 35 22.1	38816	95	2.3	*	TCG90	-52		
25865	4 30 20.6	-61 40 59.5	20007	42	6.9		fibr	1012	19987	36
			19931	93	2.6		argu			
			20340	80			MQ81b	-20		
			19806	115	3.0		TCG90	38		
28026	4 30 20.9	-61 41 33.8	80561	154	2.1	*	TCG90	-113		
27204	4 30 21.6	-62 01 42.6	18964	31	12.1		fibr	417	18993	44
			19059	46	9.2		fibr	1327		
25717	4 30 22.2	-61 35 21.5	17428	53	5		shec	717		
25668	4 30 24.9	-61 33 45.7	16510	74	3.2		argu		16461	37
			16380	50			MQ81a	2		
			16399	53	3.9		TCG90	7		
			16500	110			M082			
25411	4 30 25.3	-61 26 58.6	17003	94	2.0		argu		17003	94
			34939	82	2.2	*	TCG90	-48		
28041	4 30 25.6	-61 12 33.1	46688	185	1.6	*	TCG90	-152		
25752	4 30 26.5	-61 36 00.2	18658	40	6.2		shec	752	18644	35
			18470	80	2.3		TCG90	53		
27193	4 30 26.6	-60 40 52.6	19738	85	4	e	fibr	1001		
25578	4 30 28.9	-61 31 30.8	19216	67	4	e	fibr	415		
			42721	87	2.0		TCG90	-35		
28056	4 30 29.1	-61 33 28.4	14860	112	3.2		TCG90	294	14980	112
25637	4 30 30.0	-61 33 01.4	18273	52	2.5		argu		18315	81
			18350	99	3.8		TCG90	281		
27201	4 30 30.0	-61 04 10.8	17917	41	8.6		fibr	1317		
27206	4 30 30.3	-62 27 15.9	18445	40	7.0		fibr	1227		
25666	4 30 31.2	-61 33 55.9	18425	46	4.8		shec	666	18450	48
28058	4 30 32.0	-61 34 02.8	18444	88	2.0		TCG90	27	18564	88
25635	4 30 32.4	-61 33 01.5	17189	84	3.5		shec	635	17189	84
			35085	88	2.9		TCG90	-55		
25663	4 30 32.4	-61 33 34.9	17984	35	10.4		fibr	1318	17795	39
			17733	60	6.9		TCG9	1		
			17816	52	5.6		argu			
			17792	30	8.8		argu			
			17705	53			MQ81b			
			17652	30			C085			
			17746	50			MQ81a	1W		
			18020	150			V075			
			17907	53			G088			
			17780	110			M082			

difference between measured values is clearly larger than the internal uncertainties. This is detected by comparing the unweighted rms dispersion σ_{UW} to σ_T , defined as $\sigma_T = \sqrt{\sum_i \sigma_i^2 / (N-1)}$.

Therefore, we adopt as our criterion of anomaly σ_{UW} larger than $2\sigma_T$, in absence of any information about which measurement is correct, systematic errors should be incriminated, and the uncertainty of the weighted mean is given by

σ_W , without dividing by \sqrt{N} . Nevertheless, when the anomaly case detected had values of $\sigma_{\mu W}$ and σ_T lower than 50 km s^{-1} , we assumed $\sigma_{\mu W}$ as the uncertainty.

4. DISCUSSION

With the 309 new velocities for 229 galaxies reported here and those taken from our previous work and the literature as given in Table 1, a total of 387 galaxies have mea-

TABLE 1. (continued)

Ident.	α (1950)	δ (1950)	v_{\odot}	err	R	Ref	Id.Ref	\bar{v}_{\odot}	err
28048	4 30 32.4	-61 31 40.0	15336	134	2.5	TCG90	277	15456	134
25636	4 30 33.6	-61 33 31.9	18300	42	9.2	fibr	736	18123	45
			18094	64	3.1	TCG9	1		
			18000	80		MQ81b	1E		
			18052	25		C085			
			18025	110		M082			
			18270	84		W080			
			18030	200		V075			
25897	4 30 34.6	-61 42 23.1	17150	30	10.3	fibr	737	17149	30
			17142	104	3.0	argu			
			17740	70		MQ81b	-		
28053	4 30 35.1	-61 35 25.1	18396	124	2.8	TCG90	286	18516	124
27216	4 30 35.5	-61 05 04.0	17787	43	9.3	fibr	739		
27218	4 30 35.6	-60 54 09.5	5312	48	4	e fibr	1305		
25612	4 30 36.2	-61 32 45.0	20630	40	8.2	shec	612		
25633	4 30 37.2	-61 32 50.4	15846	31	6	shec	633		
25746	4 30 37.2	-61 36 25.6	15810	33	12.1	fibr	1013	15819	30
			15818	80		MQ81a	3		
			15757	76		G088			
			15756	54	3.9	TCG90	4		
			15890	110		M082			
			15777	87		W080			
27208	4 30 37.9	-61 38 09.8	15822	73	3.4	fibr	738		
27219	4 30 38.5	-60 52 15.9	5308	30	5	e fibr	1306		
25539	4 30 39.5	-61 30 38.0	14168	39	8.3	fibr	1015	14152	60
			13991	50	6.2	argu			
			14258	62		G088			
			13991	63	3.1	TCG90	3		
			14445	89		MQ81b	12		
25686	4 30 40.0	-61 34 59.5	10038	82	2.4	argu		10038	82
			27235	87	2.0	* TCG90	-28		
26009	4 30 40.8	-61 47 24.5	17565	42	8.2	fibr	1014	17564	30
			17505	62	3.0	argu			
			17610	50		MQ81b	14		
			17407	234		G088			
27209	4 30 42.9	-61 35 26.4	16642	30	9.5	fibr	414	16647	30
			16664	55	3.9	shec	712		
			63845	81	2.2	TCG90	-29		
25658	4 30 43.5	-61 33 46.3	17774	49	6.4	shec	658	17774	49
			19103	77	2.2	TCG90	-289		
25608	4 30 45.6	-61 32 15.2	18809	54	5.9	shec	608	18809	54
			27002	98	2.1	TCG90	-32		
27210	4 30 46.9	-61 29 20.1	15768	66	3.6	fibr	413		
28001	4 30 49.7	-61 32 07.6	65264	114	1.3	* TCG90	-33		
25050	4 30 51.9	-61 13 28.4	17293	185	1.7	argu		17627	98
			17480	175		MQ81b	24		
			17581	71	5.6	TCG90	150		
27207	4 30 51.9	-61 45 03.9	19397	122	2.9	TCG90	231	19517	122

sured velocities. These are distributed over nearly $2^{\circ} \times 2^{\circ}$ centered on A3266 (a projected square with $\approx 11h_{50}^{-1}$ Mpc per side). A preliminary question to be dealt with is whether the selection process of fiber positions could have spatially biased the velocity distribution. Figures 8 and 9 show the distributions of all measured positions and all measured velocities. No obvious bias is visible, confirming a homoge-

neous coverage. We should emphasize that the central coverage goes deeper than the rest of the cluster, because of the use of the 4m prime focus plate to measure positions there and the few, successful, deeper Argus velocities (intended to clarify the presence of the central dynamical cusp, as suggested in QR90). Below we present a first analysis of the velocity data, leaving for a future publication a discussion of

TABLE 1. (continued)

Ident.	α (1950)	δ (1950)	v_{\odot}	err	R	Ref	Id.Ref	\bar{v}_{\odot}	err
27212	4 30 52.7	-61 14 39.2	17687	62	4.8	fibr	1316		
27213	4 30 53.8	-61 11 46.4	18634	72	3.5	fibr	1002		
25378	4 30 56.3	-61 26 20.4	7465	51	2	fibr	1236		
28055	4 30 57.7	-61 32 12.0	15002	110	3.3	TCG90	292	15122	110
25567	4 30 58.4	-61 31 34.8	17724	34	8.5	fibr	1016	17751	30
			17779	34	8.9	shec	567		
			17660	200		MQ81b	-26		
			51236	78	2.3	* TCG90	-11		
27215	4 30 58.5	-61 06 31.6	7332	51	6	e fibr	1009		
28054	4 30 59.0	-61 30 26.1	17360	102	3.6	TCG90	291	17480	102
26023	4 30 59.9	-61 48 26.4	16118	28	8.9	shec	1023	16112	30
			15953	79	5.0	TCG90	243		
27211	4 31 01.7	-61 24 25.6	20947	51	5.5	fibr	1235		
25281	4 31 02.3	-61 23 28.7	21380	33	7.4	shec	281		
25804	4 31 03.0	-61 37 57.4	19	58	5.5	argu	-	19	30
			63752	112	1.3	* TCG90	-40		
28045	4 31 03.3	-61 36 38.4	18177	84	4.6	TCG90	234	18297	84
25535	4 31 07.3	-61 31 11.4	20512	44	6.4	shec	535	20512	44
			87647	114	1.3	* TCG90	-24		
25491	4 31 07.6	-61 29 04.2	14426	82		G088		14426	82
			39159	104	1.8	* TCG90	-36		
25601	4 31 09.0	-61 32 34.9	18921	45	8.1	fibr	1214	18864	38
			18845	60		MQ81b	23		
			18673	56	3.7	TCG90	10		
25775	4 31 10.9	-61 37 03.7	17308	60	5.3	fibr	1017	17387	61
			17337	59	5.6	shec	775		
			17300	150		MQ81b	22		
			17437	65	3.0	TCG90	9		
28000	4 31 11.7	-61 31 54.9	74512	94	1.8	* TCG90	-23		
28040	4 31 12.9	-61 14 43.9	18366	138	2.4	TCG90	-147		
25709	4 31 15.1	-61 35 26.8	19471	35	7.3	shec	709	19492	40
			19450	66	3.0	TCG90	25		
25323	4 31 16.6	-61 24 45.0	17773	43	5.3	argu		17681	68
			17631	32		G088			
			17420	110		MQ81a	-6		
25061	4 31 17.8	-61 14 16.8	17355	37	8.9	fibr	1008	17370	39
			17310	50		MQ81b	18		
			17341	51	8.2	TCG90	146		
27223	4 31 18.0	-61 12 40.7	17574	64	3.9	fibr	1201		
25599	4 31 18.6	-61 32 14.4	19488	41	6.7	argu		19500	34
			19411	64	3.1	TCG90	22		
25489	4 31 20.4	-61 29 29.7	17462	47	5.7	argu		17511	47
25403	4 31 20.9	-61 26 51.1	18336	39	7.9	fibr	1018	18341	30
			18350	50		MQ81b	16		
			27149	96	2.2	* TCG90	-46		
25373	4 31 22.4	-61 26 03.2	16100	30	10.4	fibr	1213	16099	30
			16090	110		MQ81b	17		
27225	4 31 22.7	-61 58 26.4	16805	33	7.9	fibr	1326		

photometric CCD data and modelling of the cluster (Flores *et al.* 1996).

4.1 Membership

The complete velocity histogram is shown in Fig. 10 in bins of 500 km s⁻¹. The cluster concentration apparently extends from 13 500 to over 25 000 km s⁻¹. A few isolated galaxies appear in the foreground between 5000 and 10 500

km s⁻¹, well separated in velocity from the cluster peak. These galaxies do not appear concentrated on the plane of the sky; only 2, at 7000 and 10 000 km s⁻¹, are seen projected in the central regions of the cluster. Towards the high velocity tail, the edge of the cluster is less well defined, where the slightly asymmetric tail could extend to 25 000 km s⁻¹ (as discussed below). One weak high velocity peak can be distinguished, between 27 500 and 30 000 km s⁻¹.

TABLE 1. (continued)

Ident.	α (1950)	δ (1950)	v_{\odot}	err	R	Ref	Id.Ref	\bar{v}_{\odot}	err	
27222	4 31 23.1	-61 09 36.2	18525	35	9.1	fibr	715			
27228	4 31 24.2	-62 21 43.4	18546	35	10.5	fibr	1226			
28046	4 31 25.9	-61 38 23.9	17862	138	2.4	TCG90	-235			
25161	4 31 32.2	-61 18 48.2	17856	48	5.4	fibr	1202	17909	84	
			18195	90		MQ81b	-19			
			17923	76	5.2	TCG90	145			
27224	4 31 36.7	-61 48 06.9	19158	40	7.5	fibr	418	19137	61	
			18833	119	3.0	TCG90	241			
28009	4 31 37.1	-61 33 38.5	77629	161	1.9	*	TCG90	-89		
25739	4 31 37.4	-61 36 07.2	18306	38	5.6	shec	739			
28005	4 31 38.8	-61 25 36.8	16969	156	2.0	TCG90	-68			
28010	4 31 41.1	-61 32 42.7	47390	199	1.4	*	TCG90	-90		
25159	4 31 44.0	-61 18 21.7	19580	42	7.8	fibr	1007	19583	58	
			19505	50		MQ81b	13			
			19629	71	5.7	TCG90	143			
27233	4 31 45.1	-60 57 52.2	33464	32	6	e	fibr	1307		
25482	4 31 45.2	-61 29 00.3	17020	64	5.5	shec	482	16914	54	
			16767	33	7.6	TCG90	43			
27227	4 31 45.8	-62 20 38.5	17456	53	5.7	fibr	1225			
28031	4 31 45.8	-61 29 35.5	17078	159	2.0	TCG90	-123			
25181	4 31 46.4	-61 19 07.4	18138	27	11.0	fibr	412	18129	30	
			18130	30	10.9	fibr	714			
			17937	76	5.2	TCG90	142			
28030	4 31 48.9	-61 29 52.2	18891	84	3.3	TCG90	122	19011	84	
28029	4 31 49.9	-61 29 18.9	17505	144	2.3	TCG90	-121			
25773	4 31 50.6	-61 36 58.9	16200	52	5.7	argu		16196	61	
			16055	100		MQ81a	7			
			16363	113		G088				
25207	4 31 53.6	-61 20 14.3	17430	224	5	e	fibr	1006	17304	57
			17291	66	2.6	argu				
			17194	139	2.4	TCG90	141			
27231	4 31 55.3	-61 44 53.3	19456	66	4.0	argu		19491	45	
			19402	62	4.8	TCG90	240			
25875	4 31 57.3	-61 41 25.8	16305	31	9.3	fibr	716	16305	31	
			26637	117	3.1	TCG90	-238			
25372	4 31 57.6	-61 26 12.4	17668	37	6.8	shec	372	17691	56	
			17707	88	4.4	TCG90	67			
25593	4 32 00.5	-61 31 56.7	16903	59	4.8	shec	593	16899	48	
			16772	83	4.7	TCG90	42			
27229	4 32 01.5	-62 26 54.9	18557	59	4.1	fibr	1224			
28036	4 32 01.9	-61 29 18.9	17234	149	2.2	TCG90	-124			
25264	4 32 04.6	-61 22 40.8	-240	103	4	e	fibr	-1005		
			22729	129	2.7	TCG90	-126			
28004	4 32 07.2	-61 27 26.2	17908	173	1.7	TCG90	-66			
28033	4 32 08.4	-61 26 02.4	63524	163	1.9	TCG90	-119			
27235	4 32 10.7	-61 04 12.6	42513	122	2.4	e	fibr	713		
28034	4 32 11.3	-61 26 19.8	18128	77	2.2	TCG90	-120			
25223	4 32 14.4	-61 20 46.8	18611	44	6.2	argu				

However, again no spatial clustering is obvious. Three galaxies are also identified at velocities between 41 000 and 42 000 km s⁻¹. No foreground or background cluster is detected out to 50 000 km s⁻¹.

In Fig. 11 we show the velocity histogram of the possible cluster members, binned in 200 km s⁻¹. Here, an extended tail to high velocities has three galaxies at 23 000 km s⁻¹. Several criteria could be applied to eliminate galaxies that

could belong to outlying groups or appear projected on the cluster which, because of its high dispersion and high velocity tail, is a non-negligible possibility. The standard iterative 3 σ clipping (Yahil & Vidal 1977) eliminates all galaxies closer than 15 000 km s⁻¹ and all galaxies beyond 21 000 km s⁻¹. However, these methods are more appropriate for rather incomplete velocity data. For numerous velocities and a wide area coverage, a more physical constraint can be ap-

TABLE 1. (continued)

Ident.	α (1950)	δ (1950)	v_{\odot}	err	R		Ref	Id.Ref	\bar{v}_{\odot}	err
25591	4 32 14.7	-61 32 00.9	15216	31	8.8		fibr	1212	15216	31
			51258	158	2.0	*	TCG90	-87		
28037	4 32 15.0	-61 24 51.8	18399	140	2.4		TCG90	-125		
25349	4 32 15.4	-61 25 23.4	16366	36	9.2		fibr	1315	16327	38
			16342	30	9.2		shec	349		
			16086	52	8.0		TCG90	57		
28038	4 32 15.7	-61 16 39.8	17535	160	2.0		TCG90	-140		
27237	4 32 16.4	-61 21 45.4	7475	50	5	e	fibr	411		
25452	4 32 16.7	-61 28 13.3	18355	45	6.7		fibr	1211	18370	37
			18283	66	3.5		TCG90	65		
25590	4 32 18.3	-61 32 00.3	17619	47	6.4		shec	590	17698	74
			17648	44	4.6		TCG90	61		
25422	4 32 18.6	-61 27 50.1	20788	60	5.3		shec	422	20856	98
			20878	86	4.5		TCG90	78		
25734	4 32 19.3	-61 36 18.0	17326	40	7.5		fibr	1210		
27238	4 32 19.4	-61 59 54.6	16707	64	3.9		fibr	728		
25450	4 32 25.3	-61 28 47.3	16115	39	8.5		fibr	410	16102	34
			15936	77	5.1		TCG90	79		
27236	4 32 25.8	-61 14 11.9	17760	36	8.4		fibr	1314		
25203	4 32 27.2	-61 19 50.5	16365	34	10.6		shec	203		
25589	4 32 27.2	-61 32 26.0	17737	32	8.7		argu		17741	30
			17627	37	5.7		TCG90	60		
25421	4 32 28.7	-61 27 27.3	17760	67	3.7		fibr	1019	17746	45
			17724	89	2.6		argu			
			17625	85	4.5		TCG90	80		
25157	4 32 32.1	-61 18 13.4	20250	76	3	e	fibr	1203	20261	61
			20285	107	2.4	e	fibr	1313		
			20185	165	2.0		TCG90	-138		
28035	4 32 34.1	-61 28 09.7	22949	87	1.9	*	TCG90	-118		
25401	4 32 34.2	-61 26 46.3	18381	31	9.2		fibr	409	18352	87
			17963	95	4.0		TCG90	81		
28006	4 32 35.6	-61 27 55.5	18108	125	2.8		TCG90	82	18228	125
25320	4 32 36.3	-61 24 12.5	17129	49	5.5		argu		17129	44
			17013	101	3.7		TCG90	58		
28032	4 32 46.0	-61 19 53.4	59107	146	2.2	*	TCG90	-137		
25475	4 32 47.2	-61 29 05.5	16965	38	6.9		shec	475	16952	33
			16786	73	5.5		TCG90	59		
25533	4 32 54.0	-61 30 37.9	17940	45	4.5		argu		17945	40
			17852	96	3.9		TCG90	63		
27253	4 32 54.7	-61 04 41.4	18421	58	5.6	e	fibr	1312		
27243	4 32 55.8	-61 22 00.1	19406	115	3.6	e	fibr	712		
28003	4 32 59.6	-61 27 11.9	20041	119	3.0		TCG90	64	20161	119
27248	4 32 59.9	-60 55 28.8	42334	74	3	e	fibr	1308		
27254	4 33 00.8	-61 17 48.8	20339	35	8.6		fibr	711		
27255	4 33 04.9	-61 29 02.0	17747	46	6.5		fibr	408	17729	46
			17484	124	2.8		TCG90	83		
27250	4 33 07.0	-60 58 42.6	17611	40	7.0		fibr	1309		
27257	4 33 08.2	-61 32 14.0	16538	30	10.4		fibr	407	16539	30

plied to take into account the combined velocity and space distributions. Galaxies with the highest relative velocities to the cluster center are expected to be projected only on the central regions, while they traverse these same regions along trajectories with angles close to the line of sight. Examination of Fig. 12, which plots the galaxy velocities in terms of the radial distance from the center, confirms this. Those galaxies within 2000–3000 km s⁻¹ of the mean velocity distrib-

ute out to large radii, but at higher relative velocities the radii get smaller, with a handful of exceptions. In fact, the present data show that the redshift caustics are fairly well defined in this cluster (Kaiser 1987). We use this fact to eliminate from our analysis two outlying galaxies from the locus of the redshift-radius area, assuming they are nonmembers or galaxies not bounded to the system (Nos. 27299 and 27336). Also, to avoid cutting off, somewhat arbitrarily, the small

TABLE 1. (continued)

Ident.	α (1950)	δ (1950)	v_{\odot}	err	R	Ref	Id.Ref	\bar{v}_{\odot}	err
			16525	34	8.9	fibr	1209		
			16478	64	6.4	TCG90	62		
28047	4 33 08.7	-61 41 31.3	11946	113	3.2	TCG90	249	12066	113
28039	4 33 10.8	-61 29 22.5	19783	76	2.3	TCG90	-117		
27246	4 33 12.2	-60 55 14.5	17715	70	4.8	fibr	1003		
27247	4 33 12.2	-60 55 20.3	17654	52	6.3	fibr	701		
28008	4 33 13.1	-61 28 35.0	17077	65	2.8	TCG90	84	17197	65
27252	4 33 15.4	-60 59 07.9	17465	69	5.9	fibr	401		
27262	4 33 16.1	-62 22 50.8	5818	78	6	e fibr	424		
27260	4 33 22.8	-61 55 46.3	16120	86	3.1	e fibr	1325		
27256	4 33 28.9	-61 29 01.5	18635	52	5.3	fibr	717		
27259	4 33 28.9	-61 35 45.9	17269	66	3.5	fibr	1020		
27273	4 33 34.7	-61 22 29.9	17611	33	8.2	fibr	710		
27276	4 33 34.9	-60 54 23.4	29462	80	3.6	e fibr	702		
27269	4 33 35.7	-61 40 13.3	16901	42	6.9	fibr	406		
27270	4 33 37.8	-61 38 21.4	16750	42	7.5	fibr	1319		
27267	4 33 38.6	-61 48 09.8	41280	37	8.2	fibr	727		
27278	4 33 41.2	-60 44 54.2	5239	78	5	fibr	1004		
27268	4 33 41.9	-61 40 57.8	17431	37	8.2	fibr	1320		
27281	4 33 57.6	-61 07 20.9	17706	288	2	fibr	402		
27280	4 33 58.6	-61 00 15.1	17581	65	3.8	e fibr	703		
27271	4 33 59.3	-61 39 17.2	17689	52	6.5	fibr	718		
27284	4 34 01.8	-61 31 15.6	17365	79	5	e fibr	405		
27279	4 34 03.5	-60 41 27.7	17593	40	6.6	fibr	704		
27265	4 34 05.9	-62 08 46.8	18516	27	9.9	fibr	423		
27286	4 34 06.3	-61 51 34.3	16848	31	9.2	fibr	726	16863	30
			16885	36	8.6	fibr	1324		
27288	4 34 08.3	-62 01 25.4	17330	51	4.8	fibr	419		
27289	4 34 09.8	-62 21 43.0	17756	79	3	e fibr	1223		
27263	4 34 12.5	-62 27 44.5	18723	40	7.6	fibr	1222		
27283	4 34 16.2	-61 30 17.9	15844	26	11.5	fibr	719		
27285	4 34 17.8	-61 39 59.9	29377	90	6	e fibr	404		
27294	4 34 28.8	-61 42 12.3	17365	47	5.4	fibr	420		
27297	4 34 32.0	-61 29 58.8	60	37	6.7	fibr	-1321		
27298	4 34 34.5	-61 11 49.3	18476	37	9.5	fibr	1311	18476	37
			17075	100	2	fibr	-709		
27299	4 34 38.5	-61 02 38.0	21102	66	5	e fibr	403		
27300	4 34 44.9	-61 02 49.9	18458	35	8.2	fibr	708		
27293	4 34 51.9	-61 42 32.2	7539	115	6	e fibr	1322		
27290	4 34 54.4	-62 27 20.6	18595	36	7.0	fibr	1221		
27301	4 35 00.8	-61 15 54.5	16994	38	6.8	fibr	707	16985	30
			16975	39	6.8	fibr	1204		
			16986	46	5.8	fibr	1310		
27302	4 35 04.5	-61 52 42.4	16824	32	9.6	fibr	421		
27303	4 35 24.1	-61 56 27.3	17711	28	9.6	fibr	422		
27306	4 35 26.2	-62 26 13.7	18436	35	8.2	fibr	1220		
27304	4 35 31.2	-62 08 31.3	17637	43	6.5	fibr	725	17639	31
			17642	45	6.3	fibr	1323		

radii high velocity tails of the distribution, expected in a numerous sample, we have retained two galaxies between 14 100 and 14 500 km s^{-1} , and one between 21 000 and 21 500 km s^{-1} (namely, Nos. 25539, 25491, and 25281), keeping 317 galaxies as cluster members. The few outliers, at large radii, could belong to loose groups falling into the cluster, or be the tail end of the tidal arm discussed later. Moreover, some other galaxies, not eliminated but close to

the locus limit, could be members of these groups or tidal arm.

4.2 Magnitude Limit

To get a rough estimate of the completeness of the velocity sample, lacking at this point wide area photometric data, we can use (our unpublished) photographic photometry of

TABLE 1. (continued)

Ident.	α (1950)	δ (1950)	v_{\odot}	err	R	Ref	Id.Ref	\bar{v}_{\odot}	err
27329	4 35 51.0	-61 32 44.7	17863	55	4.5	fibr	1208		
27308	4 35 59.4	-62 17 09.4	17738	69	5.3	fibr	1219		
27330	4 36 12.8	-61 54 22.6	17120	29	11.3	fibr	1215		
27310	4 36 19.1	-61 20 12.8	17252	40	8.0	fibr	706		
27318	4 36 44.5	-61 23 39.7	20091	55	5.2	fibr	705		
27328	4 36 49.3	-62 04 12.2	17283	43	6.5	fibr	724		
27315	4 36 51.3	-61 12 13.7	19921	70	3.9	fibr	1205		
27324	4 37 06.2	-62 12 01.4	17433	43	5.8	fibr	1218		
27322	4 37 08.4	-61 56 07.1	16743	38	7.1	fibr	723		
27326	4 37 16.7	-62 19 32.5	17645	50	6.4	fibr	1217		
27323	4 37 18.7	-61 58 50.5	16975	30	9.9	fibr	722		
27336	4 37 18.8	-61 27 38.8	15351	26	10.9	fibr	720	15306	115
			15156	48	6.0	fibr	1207		
27337	4 37 18.8	-61 07 17.6	17186	48	4.6	fibr	1206		
27331	4 37 38.9	-62 01 14.9	17604	44	7.1	fibr	1216		
27335	4 37 39.0	-61 38 45.7	17297	37	7.9	fibr	721		

References for Table 1.

This paper: argu = ARGUS spectra; fibr = LCO fiber spectra; shec = re-measured Quintana and Ramírez (1990).

Others: C085 = Carter *et al.* (1985); G088 = Green *et al.* (1988); M082 = Materne *et al.* (1982); Q81a = Melnick and Quintana (1981a); Q81b = Melnick and Quintana (1981b); TCG90 = Teague *et al.* (1990); V075 = Vidal (1975); V080 = West and Frandsen (1981).

the central 40 arcmin diameter region, obtained by PDS scans of a CTIO 4 m IIIa-J plate and calibrated by photoelectric photometry of several galaxies (Melnick & Quintana 1985). Even when photographic photometry does not give good reliable values, it is suitable to evaluate our limits, at least in a statistical sense. The histogram of the magnitudes, brighter than $m_J=20$, over the 4 m plate is plotted in Fig. 13, that also shows the histogram of the galaxies with velocities over the same area. It is evident that the velocity coverage is complete down to $m_J=17.0$, $\sim 30\%$ complete down to $m_J=17.5$, and $30\% - 50\%$ down to $m_J=18.0$, where the velocity data are sharply cut off.

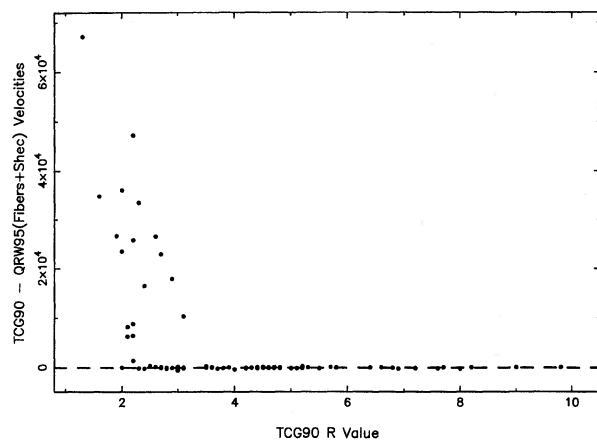


FIG. 2. Residuals of TCG90 vs QRW95 (Fibers+Schectograph) (this paper) plotted against their R value. One can see that below a TCG90 R value of ~ 2.5 we begin to differ greatly.

4.3 Velocity Dispersion

The large apparent value of the dispersion, already reported in the literature (QR90 and TCG90) could be taken as a pointer to the presence of substructure. Also, the presence of a distorted central dumb-bell could be a suggestion of a past merger of the central galaxies of two clusters (Tremaine 1990). The possibility of detecting signs of subclustering or merging can be investigated by analysing the mean and particularly, the velocity dispersion profiles (QR90). If small samples of velocities are selected at each radii, there is no

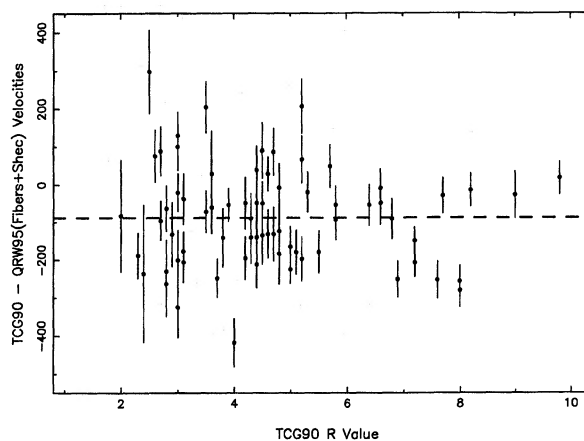


FIG. 3. Blown up section of Fig. 2 throwing out the most obvious discrepant velocities using a 3σ clipping algorithm. The velocity shift between us (QRW95 Fibers+Schectograph) and TCG90 is $\sim 100 \text{ km s}^{-1}$ with a rms 133 km s^{-1} .

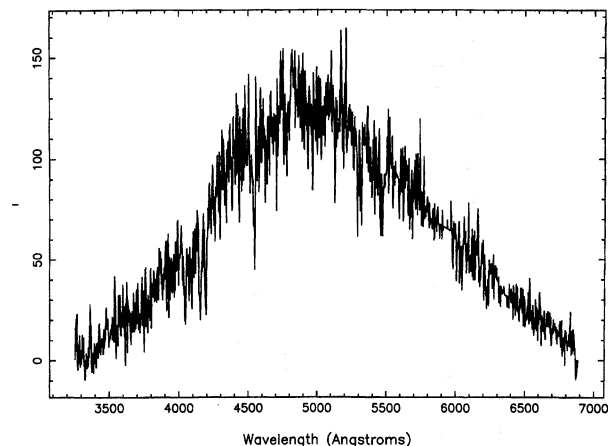


FIG. 4. Example of a spectrum with a high $R=9.54$. The usual H , K , G band and other absorption features are clearly visible. TCG90 give a velocity for this galaxy of $63\,845\text{ km s}^{-1}$ and $R=2.24$, while we obtain a velocity of $16\,642\text{ km s}^{-1}$.

reason to assume a Gaussian sample, particularly on the suspicion of substructure. Then the measurements of mean and dispersion cannot be based on an assumed Gaussian parent sample. For this reason we have used the biweighted estimators of mean location CBI (mean velocity) and scale SBI (dispersion) proposed by Beers *et al.* (1990). Unless stated otherwise, we will use these estimators throughout. In Fig. 14 we show these quantities in differential form. The data was divided in bins of 21 galaxies, enough to give good statistics and show details of the radial dependence. Both the differential scale (dispersion) and location (mean) show variations of over 2σ , with some weak correlation between them.

The mean velocity does not show a systematic change from the center to the outer edges, as expected. However, the dispersion does show a pronounced change from the central regions, with a value between 1400 and 1600 km s^{-1} , to the cluster edges, where it has fallen to 700 – 800 km s^{-1} . In fact,

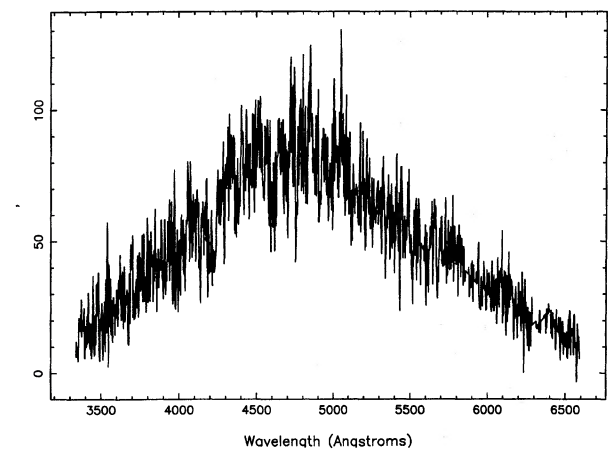


FIG. 5. Example of a spectrum with a low $R=2.12$. Absorption features are visible, though not as clear as in the previous figure. TCG90 give a velocity for this galaxy of $45\,441\text{ km s}^{-1}$ and $R=2.16$, while we obtain a velocity of $19\,595\text{ km s}^{-1}$.

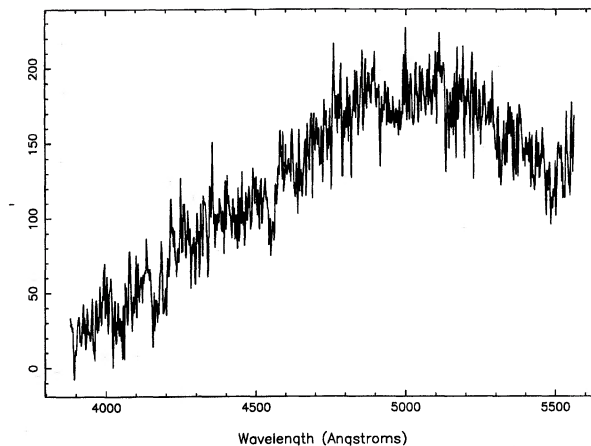


FIG. 6. An Argus spectrum with $R=4.4$ and velocity of $17\,359\pm 56\text{ km s}^{-1}$. TCG90 give a velocity of $38\,816\pm 95\text{ km s}^{-1}$ and $R=2.3$.

by $3h_{50}^{-1}$ Mpc, or one Abell radius, it has already reached this later value. This is one of the few clusters where the shape of the dispersion profile is fairly well determined, similar in shape to Coma. The dispersion decrease is both consistent with a linear decrease out to $3h_{50}^{-1}$ Mpc and constant in the outer regions, or with a smooth decreasing function that flattens at 3 – $3.5h_{50}^{-1}$ Mpc. This radial variation is consistent with the large values of the dispersion reported in the literature, derived from velocity measurements inside, or within, a projected $3h_{50}^{-1}$ Mpc. The global value for the dispersion, taking the assumed 317 galaxy members, $1085\pm 51\text{ km s}^{-1}$, using the biweight measurement, or, for better comparison with earlier values, 1131 ($-42,48$) km s^{-1} , using the standard Danese *et al.* (1980) formulas. TCG90 have applied comprehensive sets of statistical tests to their A3266 data (135 members). We will not repeat them here, in part due to the peculiarities of the velocity field presented below.

4.4 Substructure

The shapes of the velocity histogram, mean and dispersion profiles hint to the presence of clumping and substructure.

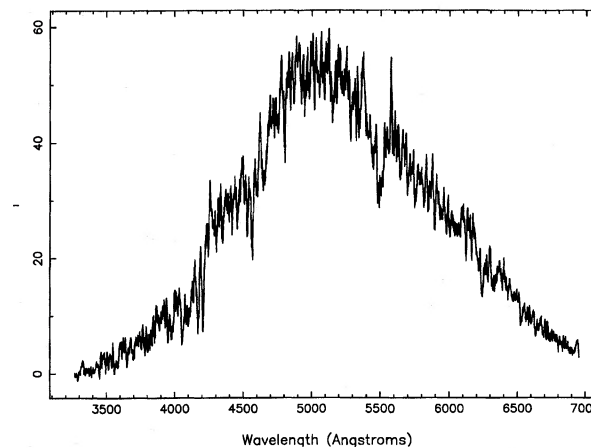


FIG. 7. A Schectograph spectrum with $R=8.3$ and velocity of $17\,995\pm 42\text{ km s}^{-1}$. TCG90 give a velocity of $44\,581\pm 72\text{ km s}^{-1}$ and $R=2.6$.

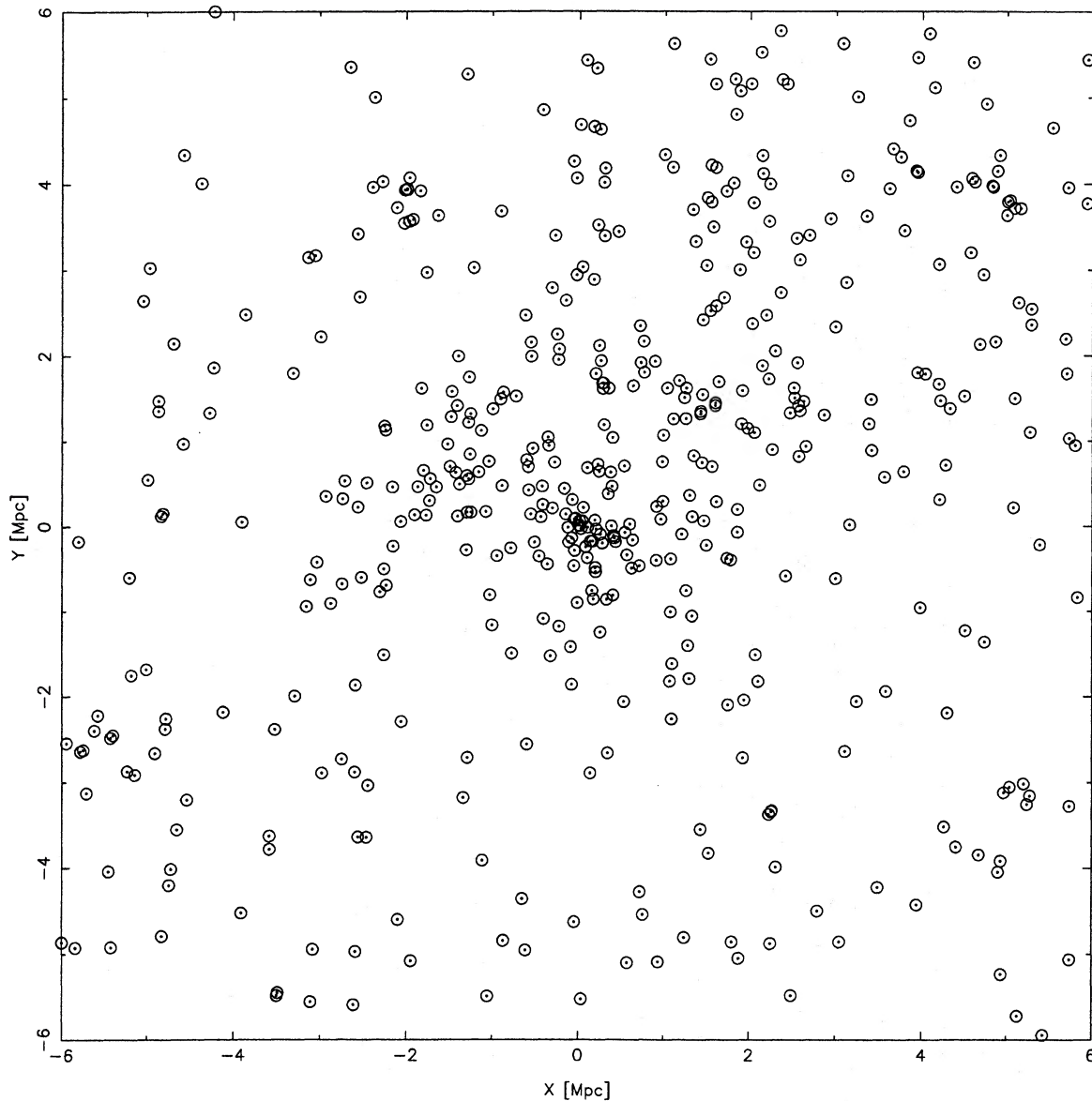


FIG. 8. Plot of the x, y positions of all galaxies with measured positions for the fiber spectrograph, identified from the ESO/Quick B Survey. Axes follow x =R.A. and y =Dec., measured in h_{50}^{-1} Mpc, with $H_0=50h_{50}$ $\text{Mpc}^{-1} \text{ km s}^{-1}$. North at top, east to left.

ture. Here we investigate the cluster velocity field. As well, a Kolmogorov–Smirnov test reveals that the velocity histogram is not consistent with a Gaussian at the 95% confidence level.

4.4.1 Substructure evidence from velocity field

Is there a connection between substructures and the profile variations in the differential mean and velocity dispersion of Fig 14? First, we note that the histogram (Fig. 11) shows two narrow secondary peaks at 17 200 and 18 400 km s^{-1} . There is an overabundance of galaxies at those speeds. It can be noted that these galaxies, if located at specific radii, could influence the mean velocity at those radii. In fact, this is seen in the mean velocity (Fig. 14), which shows two peaks reaching 18 500 and 18 300 km s^{-1} , at corre-

sponding radii of 0.5 and $2h_{50}^{-1}$ Mpc, respectively. It can be noted that only at $0.5h_{50}^{-1}$ Mpc there is a visible associated change in the dispersion, meaning the over abundant high velocity population is superimposed on the general field, increasing its dispersion. But no large change is noted at $2h_{50}^{-1}$ Mpc. Similarly, the two dips at 17 200 km s^{-1} in the velocity mean, located at 1 and $2.5h_{50}^{-1}$ Mpc radii, respectively, could be associated with the histogram peak at 17 200 km s^{-1} . However, no large effects are seen in the dispersion. To ascertain whether these features in the velocity field correspond to subgroups, we plot in Figs. 15 and 16 the space distributions of the quoted velocity peaks in 300 and 400 km s^{-1} intervals. Their projected distributions are strikingly different. In contrast, a bound subgroup would show several galaxies closely projected in space. We do not see this, with the

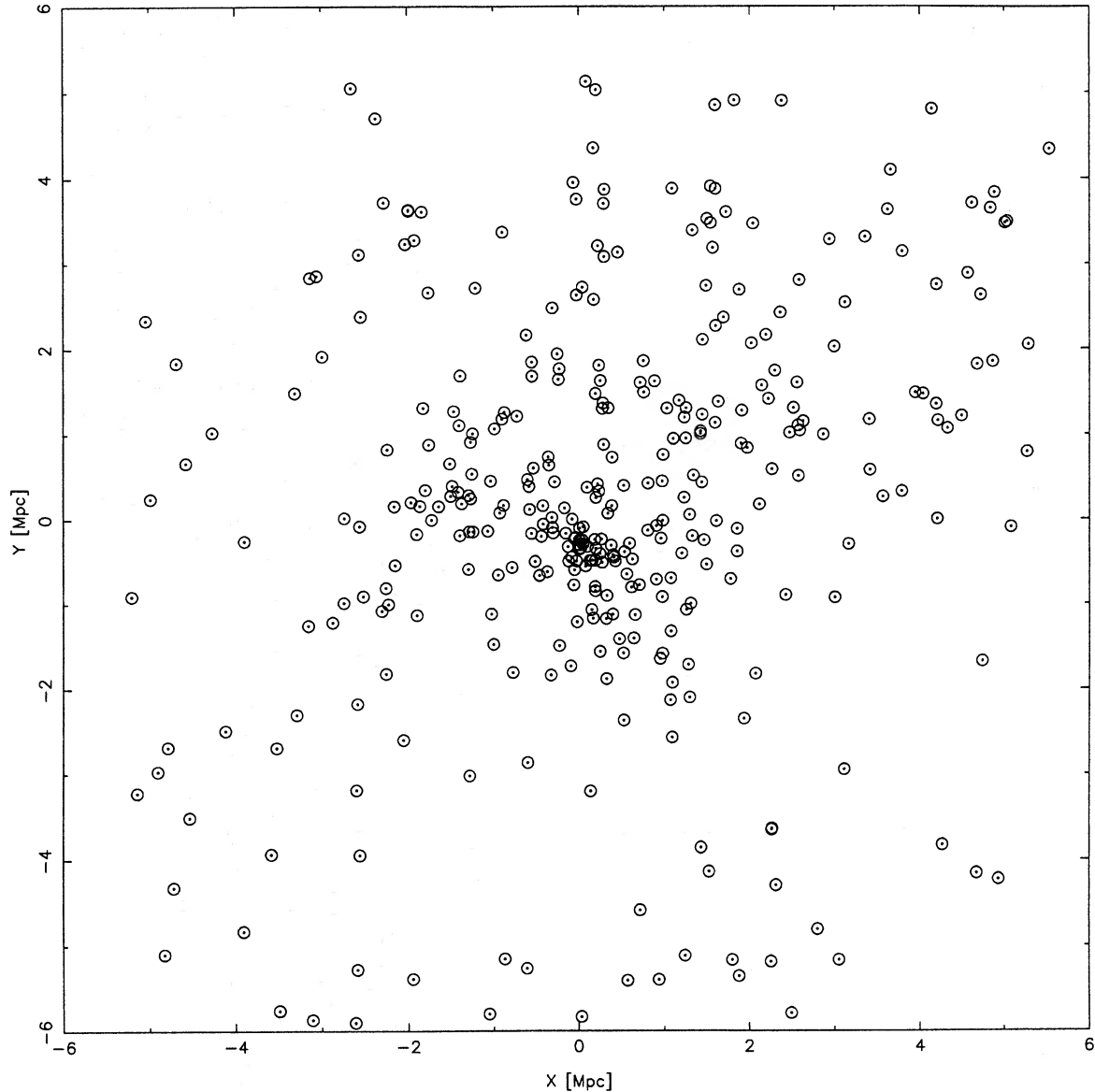


FIG. 9. Same for all galaxies with measured velocities.

possible exception of a central (higher velocity) concentration. The nature of the velocity peaks is not simple.

The different space distribution mentioned above is the more striking when we realize that it is shared by galaxies in each side of the mean cluster velocity. This unexpected distribution is shown in Figs. 17–20, where four velocity ranges, each 1500 km s^{-1} wide, are plotted. We found that, to make the separation clearer, the mean division is taken at 17500 km s^{-1} instead of 17700 km s^{-1} . The space distribution of galaxies with velocities below this mean, plotted in Fig. 17, is very spread out, fairly flat and homogeneous, with a slight E-W flattening. The distribution of Fig. 17 is markedly different from that in Fig. 19, which shows the sample 1500 km s^{-1} above the mean. Here the distribution north of the center has a wedge shape, with some clustering at the center. The velocity distribution itself may not be far from a

Gaussian, but its space distribution is far from anything symmetrical or relaxed. Furthermore, if we divide the bins into 500 km s^{-1} segments (not shown), the same features persist. Figures 18 and 20 also shows that galaxies further than 1500 km s^{-1} from the mean follows the same general pattern, but more centrally clustered (as expected from Fig. 12). Again, the higher velocity range has a tail that extends to the north. There is also a dearth of galaxies south of the center, taken at the dumb-bell position, in all plots. This could be real or due to some inhomogeneity in sampling.

Another way to look at this feature is to separate the galaxies in angular sectors. Taking as reference position angle the line joining the dumb-bell centers, in Fig. 21 we have plotted the mean velocities and dispersions, in sectors 15° wide. The third and fourth bins represent the sectors of the wedge. The superposition of all galaxies mask somewhat a

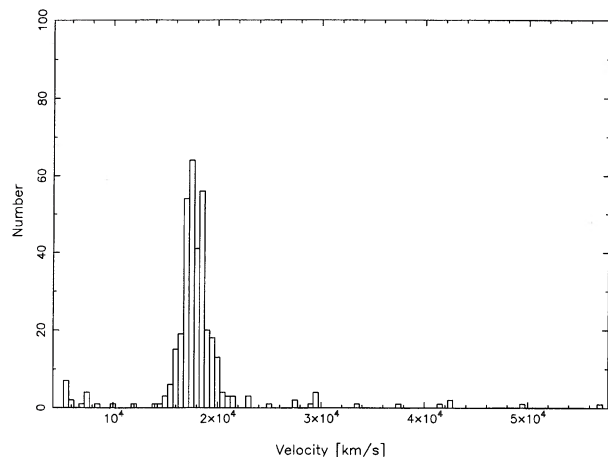


FIG. 10. Velocity histogram of all galaxies in the A3266 1.8×1.8 degree area. Bins are 500 km s^{-1} .

clear cut division, but the two mentioned bins have slightly higher velocity and low dispersions. Remarkable is that the right angle bins to the wedge have lower mean velocities.

4.4.2 Merging of two clusters

What could be the interpretation of this unusual distribution? There are basically two possibilities:

- Are we witnessing the infall from the northern side of a major infall of galaxies, sharply collimated in a wedge shape to the center by the cluster gravitational potential, or,
- Are we seeing the after effects of a merge that has produced some sort of plume, or arm, of outlying galaxies?

We first point out that, on the first interpretation above, the infall from the north should be just reaching the center, as not many galaxies of the ‘arm’ have gone through the center. Moreover, this interpretation does not lead to the formation of the dumb-bell, which should occur when the two BCMs meet.

The following evidence favours, on the other hand, a merging hypothesis:

- The x-ray emitting gas is slightly elongated in the general E-W direction (Harris *et al.* 1990 and Mohr *et al.* 1993), but close to the center it has an elongation in the

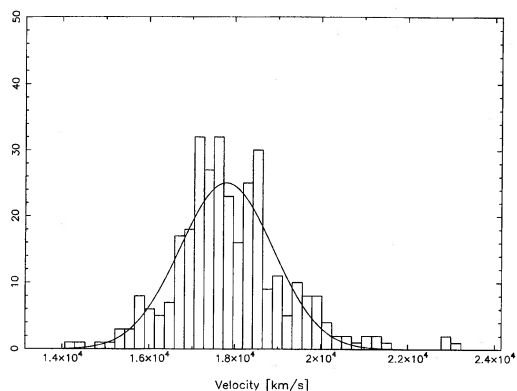


FIG. 11. Same as Fig. 10 for galaxies in the velocity range $14\,000$ and $25\,000 \text{ km s}^{-1}$, possible cluster members. Bin of 200 km s^{-1} .

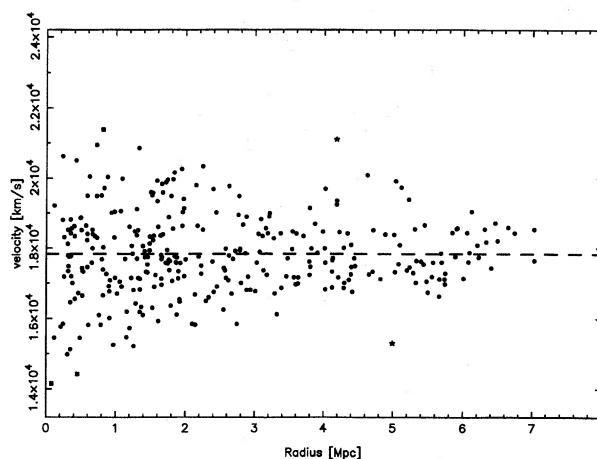


FIG. 12. Plot of velocity vs radial distance, for galaxies selected as members: circles show members selected by 3σ -clipping, squares show included members and stars show excluded members.

NE-SW direction. Hydrodynamic models should show if the gas distribution can be fitted by the merger model.

- It seems difficult to produce the dumb-bell alignment from a merger with a galaxy collapsing directly from the north. However, if the smaller cluster merged from a slightly SW direction from a position in front of the cluster the final alignment should depend on impact parameter of their brightest members (the db precursors). This picture is consistent with the NE-SW dumb-bell alignment and the x-ray structure shown in the core (see Mohr *et al.* 1993 or Fig. 22 for an optical picture of the core). The wedge shape could be produced by galaxies of the less massive core, passing thru the core of the more massive cluster. Incoming galaxies will have a distribution of velocities and impact parameters, so they could be scattered into a wide angle (as numerical models show for galaxy collisions). In fact, simulations show this to be a realistic picture and are to be described in detail in Paper II (Flores *et al.* 1996). In contrast, on the infall from the north interpretation, the wide angle of the incoming high velocity group requires that infall would be nearly radial (as

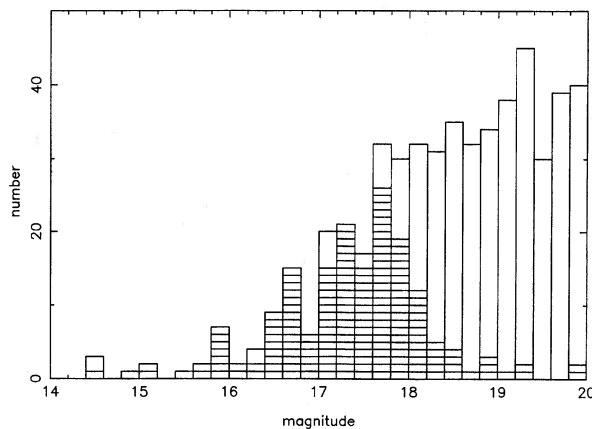


FIG. 13. Histogram of galaxy magnitudes inside a circle 40 arcmin in radius centered on the db. Filled bars show histogram of galaxies with velocities in same area.

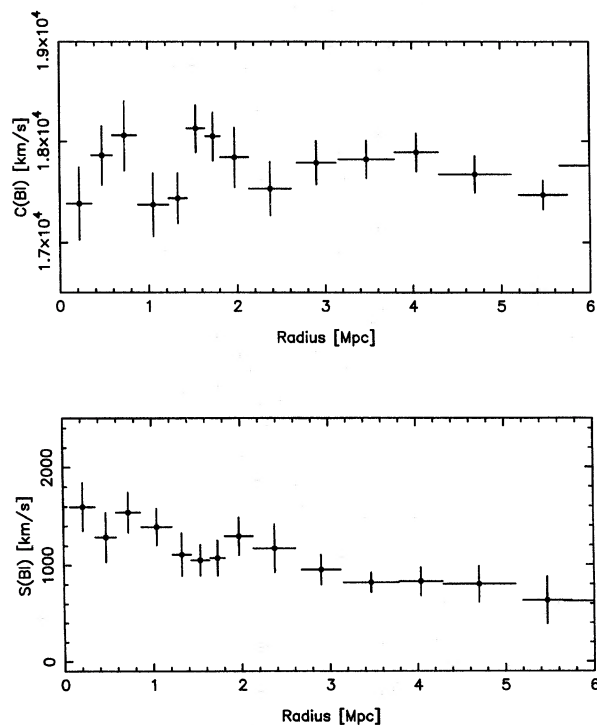


FIG. 14. (a) Radial dependence of the mean velocity, binned in rings of 21 galaxies. (b) Profile of the radial dependence of the velocity dispersion, binned in rings of 21 galaxies.

trajectories point to the center), with infalling galaxies coming simultaneously from places far apart, instead of from a concentrated cluster.

(3) Dumb-bells are supposed to form from a merge of the BCMs (Tremaine 1990), usually located close to clusters centers. As noted, this argues against the first alternative. Conversely, if the core of the merging cluster already has gone by the core of the target cluster, its brightest member has already collided with its opposite number and there has been time for the dumb-bell formation. Tremaine (1990) estimates that the time for critical separation of a dumb-bell pair is of order 1/3 of a Hubble time. The dumb-bell merge itself is small compared to this time, a few 10^8 yr (Borne *et al.* 1988).

(4) The velocities of the dumb-bell components are also consistent with the merging interpretation. First, we point out that the two secondary peaks in the velocity histogram (Fig. 11), would be interpreted as related to the cores of the two merging clusters. The high velocity one (mean velocity $18\,300\text{ km s}^{-1}$), which from Fig. 14 we suggest corresponds to galaxies having passed thru the main core, has 600 km s^{-1} relative velocity to the overall mean. The low velocity peak has a mean of $17\,200\text{ km s}^{-1}$, 500 km s^{-1} below the overall mean and slightly closer to it, as it would be expected if this component were more massive than the scattered one. The dumb-bell components (Nos. 25636 and 2 S666 in Table 1) have velocities of $17\,847$ and $18\,114\text{ km s}^{-1}$, with 50 km s^{-1} uncertainty, nearly symmetrically placed between the two velocity peaks (because of projection effects of the dumb-bell orbit, no better agreement can be expected).

Because of these reasons, we feel the evidence reveals the merging of two clusters, from roughly a SW-NE direction, with a relative line-of-sight velocity of 1000 km s^{-1} as seen today, past closest approach of their core regions. The cluster arriving from the SW was moving away from us and passed to the S (or SE) of the opposing core.

Therefore, from this argument, the total relative velocity of the cores should have been of order 1000 km s^{-1} . From this model we can ask if the scattered galaxies would have had time to produce the long arm in the time needed to also form the db? The velocity of a typical galaxy of the incoming cluster relative to the central galaxy of the other cluster prior to collision would be about 1000 km s^{-1} . The tidal arm reaches out to $3-5h_{50}^{-1}\text{ Mpc}$. Then, a scattered galaxy needs of order $\sim 5 \times 10^9 h_{50}^{-1}\text{ yr}$ to move to that position, consistent with the quoted critical time by Tremaine (1990). Considering the spread in velocities of incoming galaxies (up to ~ 2 times higher than the typical galaxy) we can put the epoch of the likely passage of the front edge galaxies of the incoming cluster by the center of the more massive core as $4 \times 10^9 h_{50}^{-1}\text{ yr}$ ago and the core collision at $1-2 \times 10^9 h_{50}^{-1}\text{ yr}$ ago. But the BCMs at the core centers collide somewhat later than that. This time is consistent with the quoted dumb-bell formation time of few $\times 10^8\text{ yr}$. In fact, calculations by Rix & White (1989) show that dumb-bell systems can survive many orbital periods, albeit under solid-body rotation conditions. In the absence of knowledge of the actual separation and 3D velocity, the orbital period can, typically be taken as $2 \times 10^8\text{ yr}$. In fact, the A3266 dumb-bell is developing an important envelope, not totally symmetric yet. A detailed study of the dumb-bell and its halo, to investigate whether it has reached the L3 Lagrangian point, could add constraints to the present model. We note a potential problem for this model. The original relative velocity of the dumb-bell components was of order 1000 km s^{-1} . Would it be possible to form a bound system in such a high velocity encounter? This may be feasible given that both components were originally BCM of their respective cores. Numerical models are needed to investigate this scenario and will be explored in Paper II.

This model is also consistent with a higher velocity dispersion in the central regions, as much as 1600 km s^{-1} , as tidal heating effects due to the collision are stronger there. The galaxies in the original core target are heated, acquiring a larger dispersion and a wider spatial distribution, as can be seen in Fig. 17. A finer point that could be raised is the apparent absence of the counter arm in the collision (here to the S or SW, supposedly), present in most numerical simulations of galaxy collisions. However, in unequal mass collisions, some models (of galaxies, certainly) do not show the secondary arm (Willumsen 1982, model 13). On account of the somewhat different conditions of cluster collisions, this matter deserves further research.

Corroborating evidence on the method comes from an examination of the velocity fields of those galaxies projected in the region of the tidal arm, and of those out of it, mostly in its southern half. Outside $2.5h_{50}^{-1}\text{ Mpc}$, the mean velocities of both regions separate nicely (not shown), with a difference of 900 km s^{-1} that falls at the cluster edges (with a low population). But inside that distance, both velocity means oscil-

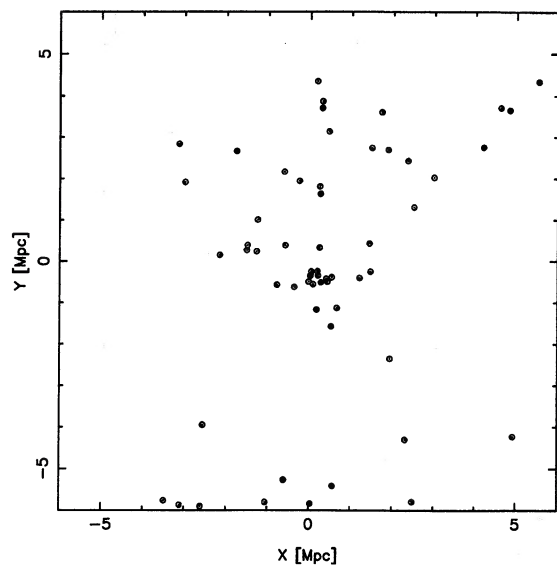


FIG. 15. Distribution on the sky of the galaxies belonging to the velocity peak centered on $18\,500\text{ km s}^{-1}$, taken 300 km s^{-1} wide.

late. Likewise for the velocity dispersions, which outwards of $2.5h_{50}^{-1}\text{ Mpc}$ have a smooth, weakly decreasing, behaviour, but fluctuate inside that radius, increasing to the center. The dispersion of the northern wedge region is consistently higher than that of the southern half. Counting superposition effects, these velocity features are indicative of the collision and, within $2.5h_{50}^{-1}\text{ Mpc}$, of ongoing violent relaxation.

4.4.3 Core substructure

Some cD dominated clusters show a central core of faint galaxies, satellite to the cD, characterized by a lower dispersion. This is interpreted as presence of a satellite system bound to the central cD (QR90; Bothun & Schombert 1988).

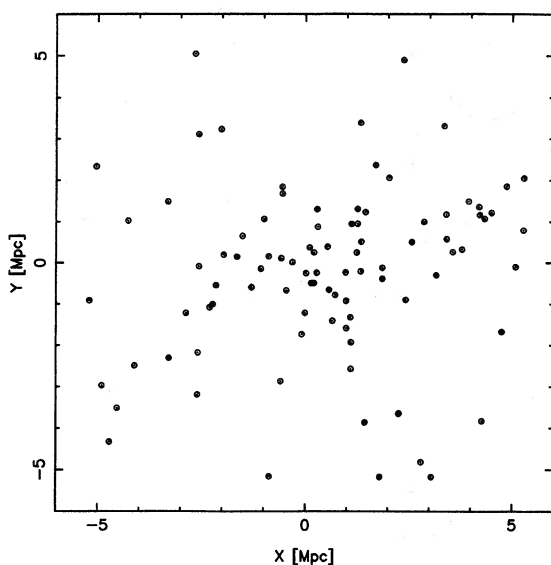


FIG. 16. Same as Fig. 15 for galaxies belonging to the velocity peak centered on $17\,200\text{ km s}^{-1}$, taken 400 km s^{-1} wide.

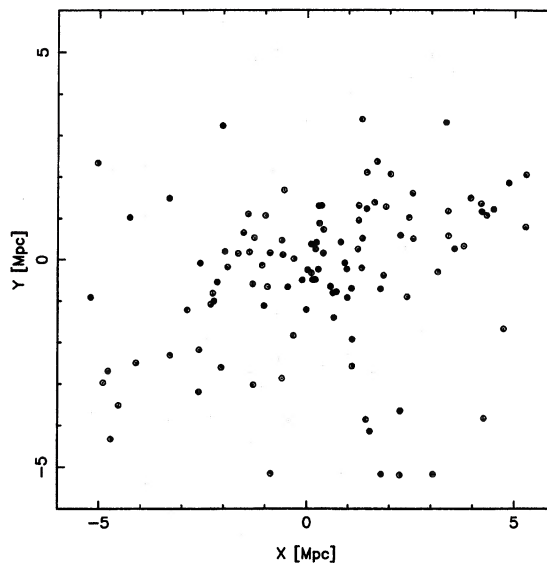


FIG. 17. Distribution on the sky of the galaxies belonging to the velocity interval $16\,000\text{--}17\,500\text{ km s}^{-1}$, i.e., in a range 1500 km s^{-1} below the mean, here taken at $17\,500\text{ km s}^{-1}$.

It was suggested (QR90) that the db in A3266 could also show such a satellite system. Although the present data do not increase much the known velocities of faint galaxies close to the db, we have three new velocities in what was defined as the cusp. The interpretation given in the previous section shows how complex matters are for the analysis of the inner regions. Taking galaxies of all magnitudes, within a given small radius, shows no significant subgroup close to the db. However, if the physical bound subsystem is formed by faint satellite galaxies (compact to be spectroscopically observable), a selection in magnitude needs to be applied. A 3σ -clipping selection of faint and compact galaxies within a

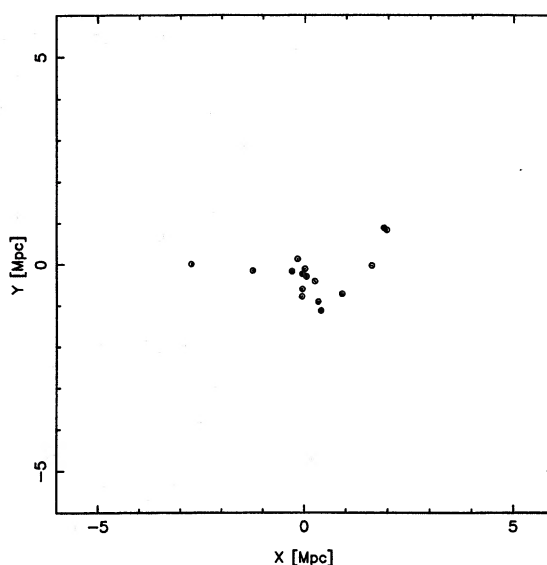


FIG. 18. Same as Fig. 17, but for velocity interval $14\,500\text{--}16\,000\text{ km s}^{-1}$, i.e., $1500\text{--}3000\text{ km s}^{-1}$ below the mean.

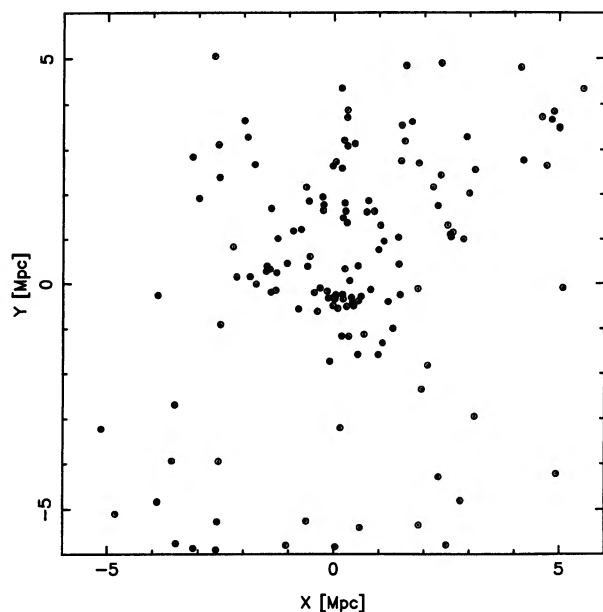


FIG. 19. Same as Fig. 17, but for galaxies belonging to the velocity interval $17\,500\text{--}19\,000\text{ km s}^{-1}$, i.e., 1500 km s^{-1} above the mean.

limiting radii of $0.4h_{50}^{-1}\text{ Mpc}$ (QR90), turns out 17 possible satellites. It should be noted that the resulting system, plotted in Fig. 23, has a flattened shape roughly aligned with the db. Its histogram is shown in Fig. 24. Three galaxies are somewhat separated from the dense velocity peak. Taking into account that some high relative velocity galaxies should, anyway, fall projected in this area, the likelihood of the satellite system stands. However, without more velocities of faint members it is hard to be more definitive. Anyhow, the velocity dispersion obtained with 19 galaxies is $647 \pm 112\text{ km s}^{-1}$ with a mean of $18\,080 \pm 154\text{ km s}^{-1}$. This low dispersion is more significant in view of the collision evidence, which should, if anything, increase the inner dispersion. We

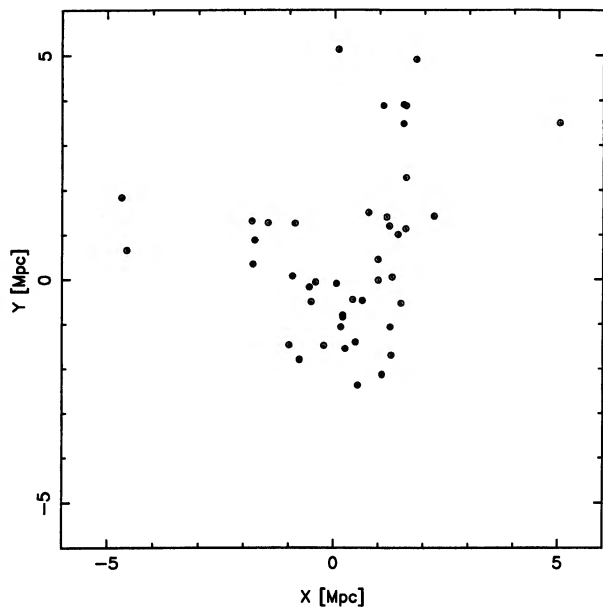


FIG. 20. Same as Fig. 17, but for velocity interval $19\,000\text{--}20\,500\text{ km s}^{-1}$, i.e., $1500\text{--}3000\text{ km s}^{-1}$ above the mean.

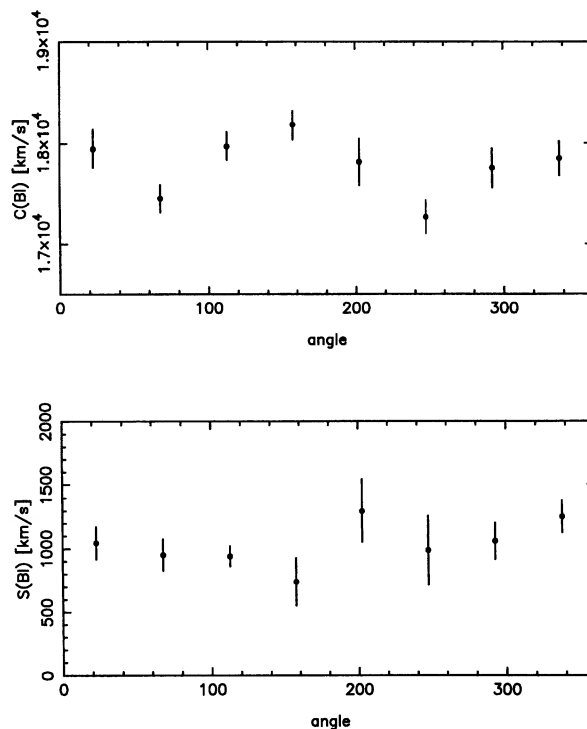


FIG. 21. Profile of the angular dependence of the (a) mean velocity and (b) velocity dispersion, binned in sectors of 45° in a counterclock direction from the axis crossing the projected dumb-bell centers.

note that the dumb-bell formation should increase, typically by a factor of 2, the depth of the central potential well, favoring the capture of satellite galaxies. The core crossing time $t_{\text{cross}} \sim 10^9\text{ yr}$, so if the two cores merged $\sim 2 \times 10^9 h_{50}^{-1}\text{ yr}$ ago $\sim (1/2)$ the cluster collision time), there was time for captured galaxies to relax, as the relaxation would occur within $2 t_{\text{cross}}$. We defer further discussion to the analysis of photometric and morphological data, needed to identify

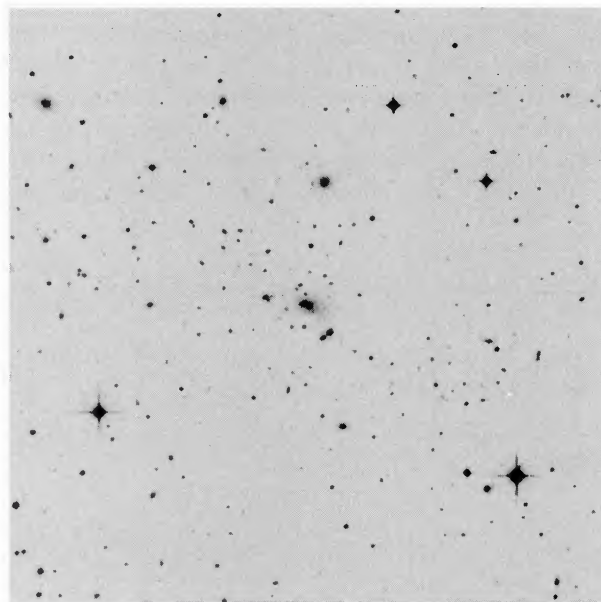


FIG. 22. Image of the central region of A3266 taken from the STScI/ASP Digitized Sky Survey on CD-ROM (approximately 15 arcmin on a side).

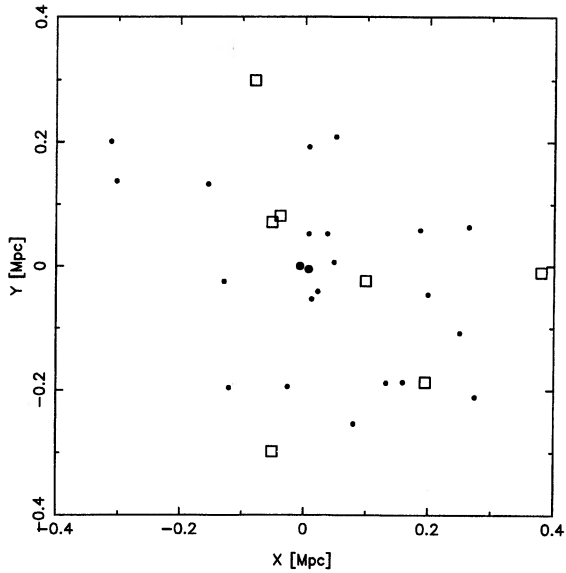


FIG. 23. Distribution of the galaxies within 400 kpc from the position of the dumb-bell. The big fill dots symbols mark the dumb-bell components, small fill dots denote faint satellites, and open squares show bright members.

probable satellites. We emphasize that CCD images of the dumb-bell show a compact system surrounding the galaxy.

4.5 Mass

The mass can be estimated using any of the usual mass estimators, given by Heisler *et al.* (1985), as discussed by QR90. The virial estimator assumes a relaxed cluster, but not other measures of mass. One can either assume a system of equal mass self gravitating particles or a massless system orbiting a point mass. Obviously, this later assumption is far from the reality in a rich cluster, but not too bad an assumption to calculate the mass of the central core system with. Table 2 gives the mass estimates obtained for the global cluster and for the 19 galaxies in the core. All the global values are quite close to one another and consistent with a total value of $5.3 \pm 1 \times 10^{15} h_{50}^{-1} M_{\odot}$. In spite of the large number of known velocities, the actual merger process indicates that mass values obtained as above are only indicative.

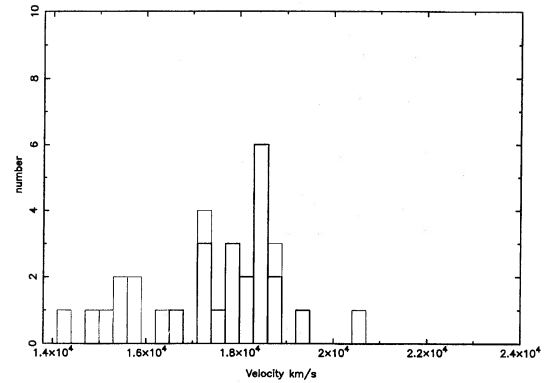


FIG. 24. Velocity histogram of galaxies in Fig. 14(a). The heavy line marks the dumb-bell and satellite's histogram. The bin size is 300 km s^{-1} .

Time-dependent models, if they can fit all the data, are needed to produce more reliable mass estimates.

5. CONCLUSIONS

We have found a velocity dispersion curve that decreases from 1500 km s^{-1} in the central regions to half that value for radii larger than $3.5 h_{50}^{-1} \text{ Mpc}$. The mean velocity does not change appreciably at different radii, but there is a slightly higher velocity at the center and northern half of the cluster. The interpretation we would like to put forward is that irregularities in the mean and dispersion radial functions (akin to a certain degree of apparent turbulence of the galaxy velocity field) are effects of a merger of two clusters coming together from a general NE-SW direction with a relative velocity of order 1000 km s^{-1} . We discovered a remarkable asymmetry in the space and velocity structures that points toward such an interpretation. The two cluster started colliding some $4 \times 10^9 h_{50}^{-1} \text{ yr}$ ago, with the central cores coming together in the last $1-2 \times 10^9 \text{ yr}$ ago and the galaxies moving from the SW going away from us, passed through the more massive core, to form the wedge shaped tidal arm, found here. This model is also consistent with the general elongation of the dumb-bell pair and with the fact that the pair had sufficient time to form. Likewise, the elongation of the x-ray emitting gas could also be consistent with the above inter-

TABLE 2. Mass estimators.

	R Mpc (1)	N (2)	MV $10^{14} h_{50}^{-1} M_{\odot}$ (3)	MP $10^{14} h_{50}^{-1} M_{\odot}$ (4)	MA $10^{14} h_{50}^{-1} M_{\odot}$ (5)	MM $10^{14} h_{50}^{-1} M_{\odot}$ (6)
A3266	7	317	52.7	51.4	51.2	46.5
	3	206	40.5	44.9	37.8	34.5
	2	166	34.6	38.9	32.1	28.8
core	0.4	19	1.8	2.3	1.4	1.5
A1656	2	165	13.7	16.0	12.7	10.5

pretation. Furthermore, the suggestion of the presence of a core of bound faint satellite galaxies of the central dumb-bell has not disappeared, but photometry, a morphological analysis and more velocities of central faint galaxies are needed to clearly elucidate this matter.

The global cluster velocity dispersion is estimated at $1085 \pm 51 \text{ km s}^{-1}$, but it should be kept in mind that it reaches large central values. This is a feature to be kept in mind on the study of other clusters, where it is claimed that 20 or 30 velocities give a good estimate of the dispersion and mass parameter (Girardi *et al.* 1993). The assumption of a global, radii-independent, Gaussian velocity dispersion, is particularly weak. The mass estimated is more than twice the mass of the Coma cluster (see Table 2), making A3266 a very massive system, as previously suggested.

Further morphological and photometric analysis can help to clarify or confirm the merger evidence and related results

of our analysis. These will be reported separately. Of special relevance are the deep x images becoming available for this cluster.

We would like to thank the Directors of the Observatories of the Carnegie Institution of Washington and the Cerro Tololo Interamerican Observatory for generous allocation of telescope time and their staff for always professional and friendly support, in particular, Stephen Sheckman for use of the fiber spectrograph, John Filhaber for help on its use a first time and night assistant A. Guerra. We also thank Tina Bird and R. Flores for helpful discussions, Tim Beers for providing the *ROSTAT* software and the anonymous referee for comments that improved the paper. M.J.W. has been supported by Research and Research Board awards at The University of Missouri St. Louis. As well, this work was partly supported by Projects FONDECYT 90/371 and 193/0572.

REFERENCES

- Abell, G. O., Corwin, Jr., H. G., & Olowin, R. P. 1989, *ApJS*, 70, 1
 Beers, T. C., Flynn, K., & Gebhardt, K. 1990, *AJ*, 100, 32
 Bird, C. M. 1994, *AJ*, 107, 1637
 Borne, K. D., Balcells, M., & Hoessel, J. G. 1988, *ApJ*, 333, 567
 Bothun, G. D., & Schombert, J. M. 1988, *ApJ*, 33, 617
 Briel, U. G., & Henry, J. P. 1993, *A&A*, 278, 379
 Carter, D., Teague, P. F., & Gray, P. M. 1981, in *Groups and Clusters of Galaxies*, edited by F. Mardirossian (Reidel, Dordrecht), p. 93
 Carter, D., Inglis, I., Ellis, R. S., Efstathiou G., & Godwin, J. G. 1985, *MNRAS*, 212, 471
 Danese, L., DeZotti, G., & di Tullio, G. 1980, *A&A*, 82, 322
 Escalera, E., Biviano, A., Girardi, M., Giuricin, G., Mardirossian, F., Mazure, A., & Mezzetti, M. 1994, *ApJ*, 423, 539
 Fairall, A. P., & Jones, A. 1991, *Southern Redshifts Catalogue and Plots*, Publications of the Department of Astronomy, University of Cape Town, No. 11
 Flores, R., Way, M., Bird, C., & Quintana, H. 1996 (in preparation)
 Girardi, M., Biviano, A., Giuricin, G., Mardirossian, F., & Mezzetti, M. 1993, *ApJ*, 404, 38
 Green, M. R., Godwin, J. G., & Peach, J. V. 1988, *MNRAS*, 234, 1051
 Harris, D., *et al.* 1990, *The Einstein Observatory Catalog of IPC X-Ray Sources*, Vol. 2 (Smithsonian Astrophysical Observatory, Cambridge, MA)
 Heisler, J., Tremaine, S., & Bahcall, J. N. 1985, *ApJ*, 298, 8
 Hoaglin, D. C., Mosteller, F., & Tukey, J. W. 1983, *Understanding Robust and Exploratory Data Analysis* (Wiley, New York)
 Hu, E., Cowie, L., & Wang, Z. 1985, *ApJS*, 59, 117
 Jacoby, G. H., Hunter, D. A., & Christian, C. A. 1981, *ApJS*, 56, 257
 Jones, C., & Forman, W. 1992, in *Clusters and Superclusters of Galaxies*, edited by A. C. Fabian (Kluwer, Dordrecht), p. 49
 Kaiser, N. 1987, *MNRAS*, 227, 1
 Kurtz, M. J., Wyatt, W. F., Fabricant, D. G., Torres, G., Kriss, G. A., & Tonry, J. L. 1992, in *Astronomical Data Analysis & Systems I*, edited by D. M. Worrall, C. Biemesderfer, and J. Barnes, ASP Conf. Ser. Vol. 25 (ASP, San Francisco), p. 132
 Materne, J., Chincarini, G., Tarengi, M., & Hopp, U. 1982, *A&A*, 109, 238
 Melnick, J., & Quintana, H. 1981a, *A&AS*, 44, 87 (MQ81a)
 Melnick, J., & Quintana, H. 1981b, *AJ*, 86, 1567 (MQ81b)
 Melnick, J., & Quintana, H. 1985, *AJ*, 89, 1288
 Miralda-Escudé, J. 1993, *ApJ*, 403, 497
 Mohr, J. J., Fabricant, D. G., & Geller, M. J. 1993, *ApJ*, 413, 492
 Pickles, A. J. 1985, *ApJ*, 296, 340
 Proust, D., Talavera, A., Salvador Sole, E., Mazure A., & Capelato, H. V. 1987, *A&AS*, 67, 57
 Quintana, H., Melnick, J., Infante, L., & Thomas, B. 1985, *AJ*, 90, 410
 Quintana, H., & Ramírez, A. 1990, *AJ*, 100, 1121 (QR90)
 Quintana, H., Ramírez, A., & Way, M. J. 1995a, *AJ* (submitted)
 Quintana, H., Ramírez, A., Melnick, J., Raychaudhury, S., & Slezak, E. 1995b, *AJ*, 110, 463
 Ramírez, A. 1994, Masters thesis, Catholic University of Chile
 Rix, H.-W. R., & White, S. D. M. 1989, *MNRAS*, 210, 941
 Salvador-Solé, E., González-Casado, G., & Solanes, J. M. 1993, *ApJ*, 410, 1
 Sheckman, S. S. 1989, *Carnegie Institution of Washington Year Book* 1989, pp. 25–32
 Tonry, J., & Davis, M. 1979, *AJ*, 84, 1511 (TD79)
 Teague, P. F., Carter, D., & Gray, P. M. 1990, *ApJS*, 72, 715 (TCG90)
 Tremaine, S. 1990, in *Dynamics and Interactions of Galaxies*, edited by R. Wielen (Springer, Berlin) p. 394
 Vidal, N. 1975, *PASP*, 87, 625
 West, R. M., & Frandsen, S. 1981, *ApJS*, 44, 329
 Willumsen, J. V. 1982, *MNRAS*, 199, 493
 Yahil, A., & Vidal, N. 1977, *ApJ*, 214, 347